1

2

3

10

11

12

13

14

15

16

17

18

19

20

21

22

23

24

25

26

27

28

29

CONTROLS OF BASEMENT FABRIC ON RIFT COUPLING AND DEVELOPMENT OF NORMAL FAULT GEOMETRIES: INSIGHTS FROM THE RUKWA – NORTH MALAWI RIFT

Erin Heilman[1]

Folarin Kolawole[2]

Estella A. Atekwana[3]*

Micah Mayle[1]

Mohamed G. Abdelsalam[1]

[1]*Boone Pickens School of Geology*
Oklahoma State University
Stillwater, Oklahoma, USA

[2]*ConocoPhillips School of Geology & Geophysics*
University of Oklahoma
Norman, Oklahoma, USA

[3]*Department of Geological Sciences*
College of Earth, Ocean, and Environment
University of Delaware
Newark, Delaware, USA

*Corresponding author email: atekwana@udel.edu

August 2018

2

73 **Highlights**

74 • To the SW, newfound strike-slip fault links the Rukwa and North Malawi Rift (RNMRS)

75 • To the NE, RNMRS border faults, intervening faults and volcanic centers are colinear

76 • RNMRS border faults and transfer structures align with pre-existing basement fabrics

77 • Basement fabrics guide the development of normal fault geometries and rift bifurcation

78 • Basement fabrics facilitate the coupling of the RMRS border faults and transfer structures

79

80

81 **ABSTRACT**

82 The Rukwa Rift and North Malawi Rift Segments (RNMRS) both define a major rift-oblique

83 segment of the East African Rift System (EARS), and although the two young rifts show colinear

84 approaching geometries, they are often regarded as discrete rifts due to the presence of the

85 intervening Mbozi Block uplift located in-between. This problem has been complicated by the

86 dominance of the Rungwe volcanic features along the northeastern boundary of the Mbozi Block

87 and lack of distinct normal faults along the southwestern boundary of the block. Here, we

88 investigate the coupling of discrete rift segments during the onset of continental rifting,

89 modulated by the control of pre-existing basement fabrics on the development of the border fault

90 geometries and linkage across the intra-rift transfer zone. We utilized the Shuttle Radar

91 Topography Mission Digital Elevation Models (SRTM-DEM) to investigate the morphological

92 architecture of the rift domains; and aeromagnetic data and SRTM-DEM to assess the

93 relationships between the rift structures and the pre-existing basement fabric (in plan-view). Our

94 results show that the present-day morphology of the RNMRS is characterized by along-rift

95 alternation of rift shoulder polarity, characteristic of coupled rift segments. Careful interpretation

96 of filtered aeromagnetic maps along the northeastern and southwestern boundaries of the

97 RNMRS reveal striking alignment of the rift-bounding faults with colinear NW-SE-trending pre-

98 existing basement fabrics. We find that rift coupling along the northeastern boundary of the

99 Mbozi Block transfer zone is accommodated by magmatism utilizing pre-existing fault systems,

100 whereas, coupling along the southwestern boundary is accommodated by a new-found dextral

101 strike-slip fault. Additionally, we show how the configuration of the pre-existing basement

102 fabrics may influence the development of rectilinear or curvilinear normal fault geometries

103 (plan-view) along the rifts, and the formation of basin-scale rift bifurcation around basement

104 inter-rift transfer zones. In summary, we suggest that the structural continuation of the boundary

105 faults along the RNMRS, and their alignment with colinear basement fabrics demonstrate the

106 influence of structural inheritance on the coupling and amalgamation of approaching rift

107 segments.

108

109

110

111

112

113

114

115

116

117

118

1. INTRODUCTION

Pre-existing basement fabrics are often major facilitators of continental rifting environments. Mechanically, they represent areas of structural weakness that can become reactivated and allow rifts to propagate preferentially along them (e.g., Daly et al., 1989). Several studies have documented the relationships between rift faults and the pre-existing basement fabrics (e.g., Wheeler and Karson, 1989; Kinabo et al., 2007, 2008; Taylor et al., 2011; Phillips et al., 2016; Kolawole et al., 2018; Siuda et al., 2018). Further, recent studies have assessed the 3-dimensional relationship between pre-existing basement thrusts and intra-rift normal faults, revealing the control of the pre-existing basement structures on the nucleation and strain distribution along the normal faults (e.g., Collanega et al., 2018). In the Cenozoic East African Rift System (EARS), which is divided into an Eastern, a Western and a Southwestern Branch (Fig. 1A), several zones of well-developed basement fabric influence rifting. One of the best recently-documented examples highlighting the influence of the Precambrian basement shear zones on rifting in eastern Africa is the role of the Mwembeshi Shear Zone on the development of the Luangwa Rift (Fig. 1A; Sarafian et al., 2018). It was demonstrated that the Mwembeshi Shear Zone acted as lithospheric conduit for fluids to migrate up the lithosphere, thus facilitating the weakening and subsequent initiation of the Luangwa rift in the Permo-Triassic.

However, the relationship between rift segments along the western branch of the EARS and the Precambrian shear zones is rather complex and warrants detailed and careful examination. For example, the Precambrian NW-trending Aswa shear zone resulted in the termination (rather than facilitation) of the northeastward propagation of the Albertine-Rhino graben which represents the northern-most segment of the Western Branch (Katumwehe et al., 2015) (Fig. 1A). On a basin scale, previous studies have also shown that pre-existing basement

142   shear zones can influence the localization of fault development (e.g., Phillips et al., 2016;

143   Kolawole et al., 2018), and in fact control fault segmentation and across-basin strain transfer at

144   later stages of rift development (e.g., Muirhead and Kattenhorn, 2018).

145   The border faults along large continental rift systems, e.g., the EARS, are typically ~100

146   km long (e.g., Foster et al., 1997; Lao-Davila et al., 2015), and the development of such large

147   normal faults with complex segment linkage styles are yet to be fully understood (e.g., Fossen

148   and Rotevatn, 2016; Gawthorpe et al., 2003; Rotevatn et al., 2018). However, since the

149   interactions between the large normal faults within juvenile extensional tectonic settings lead to

150   the systematic coupling of rift segments across transfer zones (e.g., Corti, 2012), border fault

151   segmentation, geometries and continuity between rift segments can provide insight into the

152   larger process of coupling between the segments of a rift system.

153   In this study, we focus on the Rukwa-North Malawi segment of the EARS, which is a

154   major rift-oblique segment of the rift system and serves as the central segment of the system. For

155   simplicity, we here-in refer to the Rukwa - Northern Malawi Rift segment of the East African

156   Rift as the "RNMRS". This segment is composed of the Rukwa Rift basin, the North Malawi

157   Rift basin and the Mbozi Block which represents the accommodation zone between the two rifts

158   (Fig. 1B). We address the longstanding question of the role of long-lived pre-existing basement

159   structures in the development of the trends and geometries of rift-bounding faults, leading to

160   subsequent coupling of individual rift segments during the onset of continental rifting. We

161   demonstrate that there is continuous structural connectivity along the boundaries of the RNMRS,

162   modulated by reactivation of the Precambrian metamorphic fabrics, and show that the

163   characteristic plan-view geometries of the rift-bounding faults are modulated by the

164   configuration of the basement fabric.

2. GEOLOGIC SETTING

2.1. The Precambrian Domains

The Rukwa-North Malawi Rift Segment is located within the NW-trending Paleoproterozoic Ubendian orogenic belt which is sandwiched between the Archean Tanzanian craton in the northeast and the Bangweulu cratonic block to the southwest (Figs. 2A-B; Fritz et al., 2013). The Ubendian Belt is composed of different Precambrian terranes bounded by steep shear zones (Delvaux et al., 2012). These terranes contain granulite-facies metamorphic rocks (2100-2025 Ma), amphibolite-facies metamorphic rocks and granitoids (1960-1800 Ma) that have undergone dextral strike-slip shearing and granitic plutons (1090-1120 Ma), (Fritz et al., 2013). The Paleoproterozoic Usagaran orogenic belt that extends NE-SW perpendicular to the Ubendian orogenic belt in southern Tanzania, is composed of eclogites (~2000 Ma), volcano-sedimentary cover with some low-grade metamorphism (~1920 Ma), and granitoids and granitoid gneisses (1900-1730 Ma) (Fritz et al., 2013). The Usagaran and Ubendian orogenic belts resulted from collision with the Tanzania craton, where the Usagaran orogenic belt was thrust onto the craton and the Ubendian orogenic belt was accreted along the craton's margin because of strike-slip motion (Daly, 1988; Lenoir et al., 1994). The Ubendian Belt was reactivated several times, first at ~1860 Ma as a shear zone, then again at ~800 Ma and was subsequently reactivated about every 200 Ma (Lenoir et al., 1994). Mapped shear zones along the Ubendian Belt include the ~600 km long and ~30 km-wide Mughese Shear Zone, the Mtose Shear Zone, and the Chisi Shear Zone (Fig. 2; Daly, 1988; Schenk et al., 2006; Delvaux et al., 2012). Recent studies have highlighted the role of the Mughese Shear Zone in fault development and the distribution of seismicity in Northern Malawi Rift Basin (Dawson et al. 2017; Kolawole et al., 2018).

188 *2.2. The Rukwa Rift, Northern Malawi Rift, and the Mbozi Block accommodation zone (RNMRS)*

189 The RNMRS evolved during the Permo-Triassic episode of rifting that affected southern and

190 eastern Africa, also known as Karoo rifting (Chorowicz, 2005). Outcrops of Karoo sediments

191 have been mapped along the southern end of the Rukwa Rift (Figure 2) and the northern section

192 of the North Malawi Rift Basin (Kilembe and Rosendahl, 1992). These sediments lie

193 unconformably over the Precambrian basement and consist mainly of sandstone, shale, and coal

194 and thicken towards the border faults providing evidence for reactivation of synthetic faulting in

195 the Permo-Triassic (Morley, 1992; Delvaux et al., 1992).

196   Cenozoic rifting began in the Upper Miocene, characterized by normal faulting and basin

197 subsidence with the diagenesis of Red Sandstones and Lake Bed Sediments (Delvaux and

198 Hanon, 1991). Additional subsidence occurred after the deposition of these packages, and in

199 different directions, evidenced by the drag orientations of sediment packages on the faults

200 (Kilembe and Rosendahl, 1992). The Cenozoic rifting featured the reactivation of older faults as

201 seen in seismic profiles of the Rukwa Rift in which the faults are mostly contiguous from Karoo

202 sediments to Red Sandstones to Lake Beds (Kervyn et al., 2006). The present-day tectonic

203 activity in the RNMRS consists of limited volcanic eruptions, minor seismicity in the Mbozi

204 Block region, and continued sedimentation in the Rukwa and North Malawi basins (Delvaux and

205 Hanon, 1991).

206   The present-day architecture of the RNMRS consists of the Rukwa Rift to the northwest

207 of the segment, with the Lupa Fault (generally considered the border fault) bounding it to the

208 northeast and the Ufipa Fault to the SW (Fig. 1B). Towards the southeastern end of the Rukwa

209 Rift. It bifurcates around the Mbozi Block forming the Songwe Trough (ST) to the northeast and

210 the Musangano Trough (MT) to the southwest. The Mbozi Block transitions into the North

211   Malawi Rift (also known as the North Basin) which represents the southeastern end of the

212   RNMRS and it consists of a half-graben, bounded to the northeast by the Livingstone Fault (Fig.

213   1B). The Mbozi Block is referred to as an accommodation zone because it is thought to

214   accommodate and transfer relative strain between the Rukwa and North Malawi Rift Basins

215   (Delvaux and Hanon, 1993)

216   The Mbozi is a mass of Precambrian basement that is composed of Meta-basites and

217   intermediate granulites and quartzites of the Mbozi Terrane (Daly, 1988) and is bounded to the

218   southwestern by the Mughese Shear Zone (Fig. 2B), and overlain on the northeast by the

219   volcanic deposits of the Rungwe Volcanic Province (RVP). The RVP is a ~1500 km^2 area of

220   volcanic rocks and structures that evolved ca. 9 Ma (e.g., Fontijn et al., 2012), and a strong

221   tectonic control on the localization of volcanic centers have been inferred (e.g., Fontijn et al.,

222   2010, 2012). To the northeast of the RVP, a poorly defined NE-trending rift basin occurs, known

223   as the "Usangu Basin", where Permo-Triassic to Recent sedimentary rocks overlie the

224   Precambrian basement (Mbede, 2002).

225   The crustal thickness beneath the Rukwa Rift is ~37.5 km (Kim et al., 2009), but varies

226   between ~33 km and ~39 km along the rift shoulder (Ufipa Plateau) (Hodgson et al., 2017), and

227   increases slightly to 41.1–42.1 km in the northwestern-most part of the rift where the rifting is

228   minimal. These suggest that overall, the crustal thinning beneath the rift has been minimal but

229   may be slightly more beneath the Songwe Trough (Njinju et al., 2018). Camelbeeck and Iranga

230   (1996) estimated ~42 km crustal thickness beneath the Songwe Trough. Whereas, an average

231   crustal thickness of 39 km has been estimated for the Rungwe Volcanic Province, ~37-39 km for

232   the North Malawi Rift, and 38-42 km for the Proterozoic terrains surrounding the North Malawi

233   Rift (Borrego et al., 2016; Njinju et al., 2018).

234   *2.3. Kinematics of the RNMRS*

235   The mode of opening of the Rukwa Rift – Northern Malawi Rift segment is controversial.

236   Overall, two models have been proposed. One of the models advocates for orthogonal rifting due

237   to the dominance of NW-trending pre-existing basement fabric in the region, which resulted in

238   the rotation of the E-W directed regional extension into NE-SW, thus producing NW-striking

239   normal faults (e.g., Delvaux et al., 1992; Morley, 2010; Delvaux et al., 2012). The other model

240   argues for oblique extension primarily due to the obliqueness of the rift segment to the E-W

241   directed extension, thus resulting in the development of NW-trending dextral strike-slip faults

242   (e.g., Chorowicz, 1989; Daly et al., 1989; Wheeler and Karson, 1994; Kervyn et al., 2006;

243   Mortimer et al., 2007). Both models are based on observations from only the Rukwa Rift and

244   North Malawi Rifts, and did not consider the kinematics of brittle structures along the Mbozi

245   Block accommodation zone.

246

247   **3.0 MATERIAL AND METHODS**

248   In this study, we carried out detailed mapping of exposed and buried fault segments within the

249   RNMRS. We utilized Shuttle Radar Topography Mission (SRTM) Digital Elevation Model

250   (DEM) to locate surface expressions of faults; and filtered aeromagnetic data to map the plan-

251   view trace of basement faults and metamorphic fabrics.

252

253   *3.1. SRTM DEM Data*

254   We extracted topographical profiles along the length of the rift from the SRTM DEM data to

255   investigate surface morphology of the rift segments which could provide insight into the

256   evolving nature of the rift architecture along the RNMRS.

257 *3.2. Aeromagnetic Data*

258 We combined three separate aeromagnetic surveys consisting of data acquired over northeastern

259 Zambia, southern Tanzania and Northern Malawi. The Tanzania survey was collected between

260 1977-1980 with flight height of 200 m and a flight line spacing of 1 km. The Zambia survey was

261 collected between 1973-1976 with a flight height of 150 m and a flight line spacing of 800-1000

262 m. The Malawi survey was carried out in 2013 with a flight height of 80 m, a flight line spacing

263 of 250 m. Before merging the three surveys, we first corrected for the skewness of the data by

264 reducing each of them to the magnetic pole (RTP). The RTP correction normalizes the magnetic

265 field to the magnetic field at the pole so the anomalies retain their correct strike and shape,

266 allowing the magnetic data to be interpreted as geologic structures (Baranov, 1957; Silva, 1986).

267 Afterwards, we applied upward-continuation (Henderson and Zeitz, 1949) of 120 m to the RTP-

268 corrected Malawi data, 50 m to the Zambia data in order to mathematically normalize the three

269 datasets to a 200 m observational height. We then merged the three surveys into a single

270 aeromagnetic grid file. Further, we applied the vertical derivative (VDR) filter to the merged data

271 in order to enhance magnetic gradients associated with possible basement faults and basement

272 metamorphic fabrics (Salem et al., 2008).

273   The vertical derivative edge filter has been very effective in the mapping of plan-view

274 trace of buried active faults from aeromagnetic data in different parts of the EARS (Kinabo et al.,

275 2007, 2008; Kolawole et al., 2017, 2018). Excluding the Rungwe Volcanic Province (RVP;

276 Figure 3) where volcanic materials overlie the crystalline basement, there is no information on

277 the presence of basaltic rocks along the fault segments interpreted in this study. Therefore, we

278 assume induced magnetization as the primary source of magnetization, except in the Rungwe

279 Volcanic Province (RVP) where volcanic deposits are present. However, we do not have

11

280   information on remanent magnetization in the RVP at this time. Due to the higher spatial

281   resolution of the Malawi aeromagnetic data (62 m grid cell size) compared to those covering

282   Zambia (225 m grid cell size) and Tanzania (250 m grid cell size), the magnetic anomalies are

283   most significantly better resolved in the Malawi part of the filtered aeromagnetic maps.

284

285   **4.0 RESULTS**

286   *4.1. Variation in rift morphology from topographic profiles*

287   We examined fifteen rift-orthogonal topographic profiles (spaced at 40 km) along the RNMRS

288   (Fig. 1B) to understand the overall along-strike variation in rift morphology. The investigation of

289   rift dynamics by careful analyses of the topographic structures has provided important

290   information on the subsurface architecture of rift systems (e.g., Pik et al., 2008; Wichura et al.,

291   2011; Lao-Davila et al., 2015). Our morphological assessments focus on the variation in the

292   scarp-heights (relief above the surface) of exposed normal faults along the RMNRS. This

293   provides the minimum estimate of the relative vertical displacements of the faults at the point of

294   assessment, hence the term 'exposed minimum vertical displacement' (EMVD) (Lao-Davila et

295   al., 2015).

296   Profile 1 (Fig. 3), obtained at the northern tip of the Rukwa Rift shows no pronounced

297   fault scarps, and the slight topographic high between Lake Tanganyika and Ufipa Fault

298   represents the northernmost tip of the Ufipa Plateau. In Profile 2, the surface morphology of the

299   rift shows sharp topographic gradients bounding the Rukwa Rift Valley. These topographic

300   gradients correspond to the scarps of the Ufipa Fault (600 m) and the Lupa Fault (750 m). In this

301   northern part of the Rukwa Rift, the Ufipa and Lupa Faults have comparable scarp heights, thus

302   illustrating a typical graben structure. In Profile 3, the rift structure changes into a half-graben

303 surface morphology with the Ufipa Fault having a significantly higher escarpment than the Lupa

304 Fault (~900 m difference). Profiles 4 to 7 show the same half-graben morphology for the Rukwa

305 Rift as in Profile 3; however, we observe that the Ufipa Fault scarp is much higher than the

306 topography of the Ufipa Plateau to its west along Profile 4.

307   Along Profiles 6 and 7, we observe that the Ufipa Fault scarp is lower than in the

308 northern profiles (Profiles 1-5) and that the Lupa Fault scarp is also higher than in the northern

309 profiles. In Profile 7, the Rukwa Rift splits into two basins separated by the Mbozi Block such

310 that the west basin (Musangano Trough) is bound by the Ufipa Fault to the southwest, and the

311 east basin (Songwe Trough) is bound by the Lupa Fault to the northeast. Profiles 7 to 9 shows a

312 continuous southeastward decrease in the scarp heights of the Ufipa and Lupa Faults; and

313 although the Ufipa Fault scarp is still visible south of the Mbozi Block along Profile 9, the Lupa

314 Fault scarp is significantly diminished. Profile 9 shows a gentle topographic transition from the

315 Musangano Trough to the Mbozi Block, but to the northeast of the Mbozi Block, the topography

316 spikes abruptly, representing the northern limits of the Rungwe Volcanic Province (RVP). In

317 Profile 10, the Ufipa Fault bounds what appears to be the southernmost extent of the Musangano

318 Trough, while the uplifted Mbozi – RVP domain dominates the terrain and drops off into the

319 Usangu Trough to the northeast. Profile 11 transects the northernmost tip of the North Malawi

320 Rift, where the RVP (bounded to the northeast by the Livingstone Fault scarp) represents the

321 most dominant structure in the terrain and the entire topography of the Mbozi Block and areas to

322 its southwest are relatively lower.

323   Profiles 12 and 13 illustrate half-graben morphologies for the North Malawi Rift (North

324 Basin) with the Livingstone Fault (northeast bounding fault) dominating the topography. Profile

325 14 transects the transfer zone between the North and Usisya Basins of the Malawi Rift showing

326 both the Livingstone border fault to the northeast and the Nyika Plateau to the southwest. Profile

327 15 which transects the Usisya Basin describes a half-graben surface morphology but in which the

328 rift bounding fault is located on the southwest.

329

330 *4.2. Aeromagnetic lineaments and basement fabric*

331 The RTP merged (Fig. 4A) and edge-enhanced (Fig. 4B) aeromagnetic maps over the RNMRS

332 provide a continuous plan-view image of the basement structures along the rift segment.

333 Although the Malawi part of the merged data has the highest resolution, the moderate resolution

334 of the Tanzania and Zambia parts of the data allows for considerable delineation of the trends of

335 magnetic anomalies. Overall, the areas of basement exposures exhibit high amplitude, high

336 frequency and short wavelength magnetic anomalies that delineate lineaments of interpretable

337 trends (e.g., Kolawole et al., 2018). The high frequency lineaments can be easily observed on the

338 rift shoulders of the Rukwa and North Malawi Rifts (Fig. 4B), and are commonly truncated at the

339 rift margins by the rift-bounding faults (black arrows in Fig. 4B).

340 Within the rift valleys where sedimentary rocks overlie the deeply-buried basement

341 rocks, the detailed magnetic fabric of the basement becomes suppressed such that gradients in

342 the magnetic data could correspond to fault offset within the magnetic source (e.g., Grauch and

343 Hudson, 2007, 2011; Kolawole et al., 2018) or remnants of the suppressed magnetic foliation of

344 the source (Kolawole et al., 2018). In the study area, the magnetic anomalies within the rift

345 basins are dominated by relatively lower amplitude, longer wavelength and lower frequency

346 anomalies.

347

348

14

349   *4.3. SRTM DEM Fault trends and Aeromagnetic lineaments*

350   We compare the along-axis geometry of the rift-bounding faults (from SRTM DEM) with the

351   metamorphic fabric (in plan view) of the host basement rocks along the rift shoulders (from

352   filtered aeromagnetic data) (Figs. 5-11). Figures 5-9 focus on the southwestern boundary of the

353   RNMRS, consisting of the Ufipa Fault of the Rukwa Rift, the southwestern boundary of the

354   Mbozi Block and the southwestern boundary faults of the North Malawi Rift. Whereas, Figures

355   10 and 11 focus on the northeastern boundary of the RNMRS, consisting of the Lupa Fault of

356   Rukwa Rift, the northeastern boundary of the Mbozi Block (i.e. the Rungwe Volcanic Province)

357   and the Livingstone Fault of the North Malawi Rift. We constrain our identification of the

358   Precambrian terranes and strike of their fabrics with previous field studies of the Precambrian

359   basement along the RNMRS (e.g., Daly, 1988; Wheeler and Karson, 1989; Lenoir et al., 1994;

360   Theunissen et al., 1996; Boven et al., 1999; Fernandez-Alonso et al., 2001; Ring et al., 2002;

361   Schenk et al., 2006; Delvaux et al., 2012, Lawley et al., 2013; Kolawole et al., 2018). Overall,

362   within the study area, we observe that the basement fabrics exhibit two styles, (1) discrete fabrics

363   which include isolated magnetic lineaments of strong amplitude; and (2) distributed fabrics

364   which encompass fabric sets of multiple medium-to-low amplitude magnetic lineaments as

365   distributed fabrics.

366

367   *4.3.1. Southwestern boundary of the RNMRS*

368   In the northernmost part of SW Rukwa Rift (Chisi area) (Figs. 5A-C), we observe curvilinear

369   fault geometries that follow Precambrian fabric (e.g., Ufipa, Chisi, Kalambo and Kanda Faults).

370   In the Chisi area, the Rukwa Rift border fault consists of the Northern Ufipa Fault segment and

371   the Chisi Fault segment. The tip of the Northern Ufipa Fault segment terminates against the

15

372 WNW-ESE Chisi Fault at a high angle (Fig. 5A). The Chisi Fault aligns with a strong WNW-

373 ESE magnetic-high lineament (discrete fabric) (Fig. 5B-C) known as the Chisi Shear Zone,

374 which extends eastward into the rift basin (Theunissen et al., 1996; Boven et al., 1999; Schenk et

375 al., 2006; Fig. 2B). Also, the truncated Ufipa Fault segment aligns with the Ufipa Terrane

376 basement fabrics (distributed fabrics). The North Ufipa Fault and Chisi Fault link at a very high

377 angle to form a salient that point basinward (the Chisi Salient).

378 In the central part of the Ufipa Fault (Figs. 6A-C), the fault segments also exhibit

379 curvilinear geometries and the hard linkage of major fault segments occur at high angles

380 (e.g., Kwera relay ramp). The Kwera relay ramp is the largest relay zone along the Ufipa Fault.

381 To the north of the Kwera relay ramp, the fault trends parallel to a magnetic lineament (discrete

382 fabric) that is located to its east, whereas, to the west of this fault segment, the basement is

383 characterized by two cross-cutting sets (NNW-SSE and NW-SE) of distributed fabrics. The

384 NNW-SSE set represent the fabrics of the Ufipa Terrane, but the origin NW-SE is unknown at

385 this time. The Ufipa Fault segments appear to follow the NNW-SSE basement fabrics but side-

386 steps by means of short fault segments that align with the NW-SE fabric set. To the south of the

387 relay ramp, the Ufipa Fault strikes parallel to the Mughese Shear Zone fabric which is colinear

388 with the NNW-SSE set.

389 Towards the southern part of the Ufipa Fault, in Figures 7A-C, we observe that

390 the Ufipa Fault segments exhibit rectilinear geometries such that it is difficult to delineate fault

391 bends that could correspond to breached relay ramps. In addition, we observe a stronger

392 alignment of the Ufipa Fault segments with the Mughese Shear Zone fabric within the area. To

393 the east of the Ufipa Fault, a fault that strikes parallel to the Ufipa Fault separates

394 the Musangano Trough from the Mbozi Block. The Mbozi basement is characterized by

395 metamorphic fabrics that strike WNW-ESE to NW-SE, oblique to the fault but in which subtle

396 bends in the fault trend align with the basement fabric.

397   In the southern part of the Ufipa Fault (Figs. 8A-C), the fault is characterized by two

398 segments. One of the segments represents a rectilinear southward continuation of the Ufipa Fault

399 and is bounded to the east by a linear ridge that separates it from the Musangano Trough (see

400 "Mughese Fault" segment at Tunduma in Figs. 8A-C). The other segment splays away from the

401 former and delineates a curvilinear geometry that looks like those in the northern and central

402 segments of the Ufipa Fault; this curvilinear segment bounds the southernmost part of

403 the Musangano Trough (see "Ufipa Fault" in Figs. 8A-C). Around Kaseye town (see Fig. 8A),

404 the basement is partially buried and more deeply buried around Chitipa to the south. The

405 continuation of the Ufipa Fault is only evident in the aeromagnetic data as a strong magnetic-low

406 lineament that is bounded by bands of magnetic-high lineaments (see magnetic fabrics

407 around Kaseye town in Fig. 8B). Within the Kaseye area, the NW-striking Mughese Shear Zone

408 fabrics are truncated by a discrete N-S trending magnetic-high lineament (see area within purple

409 rectangle in Fig 8C). The magnetic-low lineament that projects as a southward continuation of

410 the Ufipa Fault persists along the Mughese Shear Zone fabric into the Karonga area of the North

411 Basin of Malawi Rift where the Mughese Shear Zone is abruptly truncated by the Karonga Fault

412 (KF in Fig. 8C). The Mbozi Terrane fabric strike NW-SE, at low angles to the trend of the

413 Mughese Shear Zone.

414   Detailed analyses of the onshore faults along the hinge zone of the Northern Malawi Rift

415 (Karonga area) are well documented in Kolawole et al. (2018). Major onshore hinge zone faults

416 include the Karonga Fault (KF), St. Mary Fault (SMF), Kaporo Fault (KPF), Lupaso Fault (LF),

417 Katesula Fault (KTF) and the Mbiri Fault (Figs. 9A-C). Although the Karonga Fault cuts the

418   basement fabric, several basement-rooted buried fault segments along the rift margin align with

419   the fabric of the Mughese Shear Zone (Kolawole et al., 2018). It is interesting to note that

420   the Mbiri Fault, the longest fault (and potentially has the largest throw?) along the rift margin is

421   sub-parallel to the strike of the continuation of the Ufipa Fault into the area ("Mughese Fault" in

422   Fig. 9C). Although segments of the Mbiri Fault appear to align with the Mughese Shear

423   Zone fabic, it is not clear if the fault reactivated the southwestern boundary of the shear zone or

424   if the fault partially aligns with the fabric of the shear zone. However, we observe that for the

425   most part, the side-steps along the Mbiri Fault align with the basement fabric.

426

427   *4.3.2. Northeastern boundary of the RNMRS*

428   In the northern part of the Lupa Fault, the fault trend defines long, rectilinear segments (Fig.

429   10A) and aligns with the Katuma Terrane, similar to those observed in the southern part of

430   the Ufipa Fault where faults align with the trend of the Ufipa Terrane (Fig. 7). Although, the E-

431   W trending fabric of the Usagaran Orogenic Belt dominates the aeromagnetic data along the

432   northeastern Rukwa Rift shoulder (Fig. 10B), we also observe that closer to the Lupa Fault scarp,

433   there are some lineaments that align with the fault. To the southwest of the Lupa Fault (within

434   the rift valley), a strong magnetic-high lineament which correspond to the Chisi Shear Zone (see

435   onshore continuation and outcrop of the shear zone in Fig. 5), strike sub-parallel to the trend of

436   the Lupa Fault, but deviates more significantly southwards (Figs. 4B and 10).

437   The southern part of the Lupa Fault (between the Katuma Terrane and the Rungwe

438   Volcanic Province) is characterized by curvilinear fault segments (Fig. 10 and 11). The Lupa

439   Terrane fabrics are oriented WNW-ESE, oblique to the Lupa Fault trend (Figs. 11A-C).

440   However, subtle steps along the curvilinear fault segments align with the Lupa Terrane fabrics.

441   In the Rungwe Volcanic Province (RVP), the magnetic lineaments strike NW-SE (Fig.

442   11B), similar to those of the Mbozi Terrane (8B and C), and are truncated to the west by a strong

443   NNW-striking magnetic high lineament (white arrows in Fig. 11B). Furthermore, we observe

444   that the volcanic centers align with NNW-striking magnetic gradient superimposed on the NW-

445   striking fabrics (black arrows in Fig. 11B). South of the Rungwe Volcanic Province, segments of

446   the Livingstone Fault system describe rectilinear geometries and align with strong magnetic-high

447   lineaments (shear zone?) in the Upangwa Terrane.

448

449   **5.0 DISCUSSION**

450   *5.1. Rift architecture*

451   The present morphology of the RNMRS reflects the result of multiple episodes of rifting that

452   have affected this part of eastern Africa i.e. a Permo-Triassic rifting episode (Karoo), a

453   Cretaceous episode and the ongoing Cenozoic rifting episode (e.g., Castaing, 1991; Morley et al.,

454   1992). The Rukwa Rift has been described as both a graben (e.g., Zhao et al., 1997) and half-

455   graben (e.g., Kilembe and Rosendahl, 1992) bounded by the oppositely-dipping Ufipa and Lupa

456   normal faults. The Lupa Fault is commonly regarded as the major border fault of the Rukwa Rift

457   due to its larger throw of ~7 km (Peirce and Lipkov, 1988) relative to the Ufipa Fault (Fig. 12);

458   however, it has also been shown that the Cretaceous and Cenozoic sediments in the rift thicken

459   towards both faults (Fig. 12; Morley et al., 1992; Zhao et al., 1997). In this study, our

460   topographical assessments (Fig. 3, profiles 1-7) show that the scarp height of the Ufipa Fault

461   consistently exceeds that of the Lupa Fault through-out the rift segment, thus suggesting

462   significant footwall uplift along the Ufipa Fault.

463   The significantly lower scarp-height of the Lupa Fault suggests either that it has not been

464   very active in Cenozoic times or that it has been heavily eroded since the cessation of Mesozoic

465   rifting. However, based on these observations, we interpret that in the earlier rifting episodes

466   (especially in the Permo-Triassic Karoo episode), the Lupa Fault played the role of the major

467   border fault such that the basin defines a typical half-graben geometry; but in the present

468   Cenozoic phase of rifting, the Ufipa Fault appear to have been preferentially accommodating

469   more strain. Therefore, we suggest that the Rukwa Rift is possibly transitioning into an

470   asymmetric-graben geometry. An asymmetric-graben is a graben with EMVD greater on one

471   border fault compared to the other one, such that the basin polarity has shifted to the fault with

472   the greater 'exposed minimum vertical displacement' (EMVD) (Lao-Davila et al., 2015). The

473   implications of the present Rukwa Rift morphology on the Lupa Fault may reflect temporal and

474   spatial migration of strain accommodation from a previously dominant border fault into another

475   one that has been previously less-dominant. This could possibly be explained by the Scholz and

476   Contreras (1998) suggestion that when a rift-bounding fault attains some limiting offset, motion

477   on the fault will cease, and strain will be transferred to a new fault.

478

479   *5.2. The Southwestern Boundary of the RNMRS and relationships with Precambrian Basement*

480   *Fabric*

481   In the Chisi area, the Northern Ufipa Fault segment terminates against the Chisi Shear Zone

482   along which the Chisi Fault segment developed. The termination of the Ufipa Fault at its

483   intersection with this shear zone exemplifies one of the roles of pre-existing basement structures

484   as temporal and/or spatial mechanical 'barriers' that arrest and delimit the continuous lateral

485   propagation of a fault. Several studies on fracture propagation have demonstrated that fractures

486   are principally bifurcated, blunted, and/or arrested when they intersect discontinuities, stress

487   barriers and/or rock layers of significantly-contrasting mechanical properties along their path of

488   propagation (e.g., Helgeson and Aydin, 1991; Gudmundsson and Brenner, 2001; Zhang et al.,

489   2007; Zhang and Jeffrey, 2008). Other examples of normal fault termination at long-lived

490   basement shear zones include the case of the Albertine-Rhino Graben terminating at the Aswa

491   Shear Zone (Katumwehe et al., 2015) and the Okavango Rift border faults against the Sekaka

492   Shear Zone (Modisi et al., 2000). We suggest that both the reactivation of the Chisi Shear Zone

493   into the Chisi Fault and termination of fault segments at the shear zone demonstrate the strong

494   influence of the Chisi Shear Zone on the development of this part of the Rukwa Rift.

495   Although the northern segments of the Ufipa Fault align with the basement fabrics (Fig.

496   5B-C) and the southern segments show even stronger alignment with the NNW-SSE fabrics of

497   the Ufipa Terrane and/or Mughese Shear Zone (Fig. 7), we find that the central segments of the

498   fault show only partial alignment with this basement fabric (Fig. 6A-C). These observations

499   imply that, although the Ufipa Fault is thought to have largely propagated along the Mughese

500   Shear Zone (Fig. 2; Delvaux et al., 2012), there is stronger control of the Mughese Shear Zone

501   and Ufipa Terrane fabrics on the fault development along its northern and southern segments

502   than in the central part. We suggest that the partial control of these NNW-SSE fabrics on the

503   central Ufipa Fault segments is due to the occurrence of a NW-SE basement fabric set on the

504   Mughese Shear Zone and Ufipa Terrane fabric (Fig. 6). This may also explain the localization of

505   the largest relay zone along the Ufipa Fault at its central segment.

506   The Tunduma-Kaseye area of Malawi, through the Misuku Mountains (Fig. 8A)

507   constitute the southern boundary of the Mbozi Block. Although, the SRTM DEM shows that the

508   sub-aerial expression of the Ufipa Fault dies out roughly mid-way between Tunduma and

21

509   Kaseye, the filtered aeromagnetic data reveals that in the subsurface, the fault continues across

510   the Kaseye-Chitipa area as a distinct magnetic-low lineament that bounds the Mughese Shear

511   Zone to the south and runs southeastwards into the Karonga area (Fig. 8B). Upon closer

512   observation of the continuation of this strong magnetic-low lineament in the Kaseye-Chitipa

513   area, we find that it cuts-across and offsets a N-S striking magnetic-high lineament which

514   extends 80 km southwards into the Permo-Triassic Luangwa Rift in Zambia. We interpret this N-

515   S lineament as a mafic dike that is possibly related to one of the earlier (Triassic or Cretaceous)

516   episodes of rifting which are known to have been associated with extensive late-stage diking

517   events in the Luangwa Rift (e.g., Van de Velde and De Waele, 1998) and Shire Graben in

518   southern Malawi (Castaing, 1991). Sedimentary deposits in the Kaseye-Chitipa area resulted in

519   the burial and lack of sub-aerial exposure of this structure, thus making this study the first

520   revelation of its existence in Northwestern Malawi.

521   Our analyses of the geometry of the interpreted dike structure (Fig. 13A), here in referred

522   to as the Chitipa Dike, shows a distinct difference in the geometry of the structure to the north

523   where it is cut by the strong magnetic-low lineament (continuation of the Ufipa Fault) and to the

524   south (farther away from the fault intersection). South of Chitipa (Fig. 13B), we observe that the

525   north-trending dike describes a consistent left-stepping geometry which diminishes across the

526   Chitipa town location and continues with a more rectilinear geometry northwards into the

527   Mughese Shear Zone area. This side-stepping geometry is typical of vertical sheet intrusions and

528   are related to either magma intrusion into pre-existing stepped joint systems (e.g., Baer, 1991) or

529   near-surface stress rotations during magma intrusion (e.g., Fossen, 2010). In this study, the

530   coincidence and strike of the dike-steps along the NW- to NNW- striking basement fabric may in

531 fact suggest the possible influence of pre-existing basement fabric on the stepping geometries of

532 dike intrusions during their emplacement in host metamorphic rocks (Fig. 13B).

533 Further north, where the dike is cut by the continuation of the Ufipa Fault, the filtered

534 aeromagnetic data shows the dike exhibiting consistent right-lateral offsets across NW-SE

535 magnetic gradients (Fig. 13C). This clear distinction in the structural style of the dike south of

536 Chitipa and in the north across the continuation of the Ufipa Fault, suggest that the contrasting

537 structural styles are associated with different geological processes. In a summary, we interpret

538 that along the southern boundary of the Mbozi Block, the continuation of the Ufipa Fault, which

539 itself aligns with the Mughese Shear Zone fabric (Fig. 8B-C), is a right-lateral strike-slip fault

540 that displaced a N-S trending Mesozoic (?) dike intrusion (Fig. 13C). We further interpret that

541 this strike-slip fault reactivated the Precambrian Mughese Shear Zone at some time post-

542 Cretaceous (i.e. related to the present Cenozoic rifting phase), and therefore refer to it as the

543 "Mughese Fault". This interpretation is further supported by the change in the morphological

544 expression of the Ufipa Fault from a typical single-scarp style into a narrow linear valley-ridge

545 style in the Tunduma area in the SRTM DEM (see "linear ridge" in Fig. 8A). The observed

546 linear valley-ridge geomorphology is typical of active strike-slip fault zones (e.g., McCalpin et

547 al., 2009). In addition, previous field studies in the area (Delvaux et al., 2012) observed strike-

548 slip displacement on rock outcrops at Tunduma and Mbozi Quarry ("Q" in Fig. 8A). Using the

549 Chitipa Dike as a strain marker, we observe that the offsets increase northwards across multiple

550 splays of the Mughese Fault and estimate that the displacement is maximum at the major

551 Mughese Fault trace (northernmost extent of the strike-slip fault zone). Since mafic intrusions

552 often produce magnetic anomalies larger than the actual size of the sources, it is practically

553 impossible to estimate the true cumulative strike-slip displacement from the aeromagnetic data.

554   Based on the lateral dike separation across the fault on our aeromagnetic data, we estimate a

555   minimum of 500 m lateral displacement along the Mughese Fault (Fig. 13C). It is also possible

556   that this estimated offset only represents the lateral component of an oblique-normal slip along

557   the fault. In Figure 14, we present a conceptual model that summarizes our interpretation of the

558   Chitipa Dike geometry and the interaction of the Mughese Fault with the dike.

559   However, in Tunduma area (Fig. 8A), the presence of discrete breaching of the linear

560   ridge by stream channels suggest that the strike-slip displacement along the Mughese Fault is

561   most-likely a short-lived event that occurred at some time in the past during the development of

562   the RNMRS. The curvilinear fault scarp adjacent to the Mughese Fault at Tunduma shows

563   single-scarp morphology (not linear-ridge morphology) typical of normal faults as seen on the

564   other segments of the Ufipa Fault. Therefore, we interpret this curvilinear fault scarp as a

565   possible old segment of the Ufipa Fault that was 'pirated' by the Mughese strike-slip fault; thus,

566   suggesting a phase in which the Ufipa Fault accommodated strike-slip displacement.

567   Along the southwest margin of the North Malawi Rift (Karonga area), the Mughese Fault

568   diffuses into a zone of wide-spread faulting where the southeast-ward bend of the Mughese

569   Shear Zone controls the development of the normal faults and recent seismicity along the basin

570   hinge margin (Fig. 9A-C) (Kolawole et al., 2018; Dawson et al., 2018). Further south of Karonga

571   town, the NNW-striking Mbiri Fault is the dominant fault structure in terms of its length (and

572   displacement?) along this part of the hinge zone of the North Malawi Rift. We do not observe

573   any direct spatial connectivity between the Mughese Fault and the Mbiri Fault. However, based

574   on the sub-parallel geometry of both faults and the structural dominance of the Mbiri Fault in the

575   area, we suggest that the Mbiri Fault could possibly represent a continuation of the Mughese

576   Fault into the hinge zone of the Malawi Rift North Basin. It is also important to note that the

577   Mbiri Fault is synthetic to the Livingstone border Fault. Following the observations and

578   interpretations above, we suggest that there exists a well-developed continuous connectivity of

579   rift-related structures along the southwestern boundary of the RNMRS, facilitated by the extent

580   of the Mughese Shear Zone and the Ufipa Terrane. Interestingly, the linking of the oppositely-

581   dipping Ufipa and Mbiri Faults by the Mughese strike-slip fault describes a structure that,

582   overall, is similar to that of the Morley et al. (1990) convergent-approaching normal fault

583   system.

584

585   *5.3. The Northeastern Boundary of the RNMRS and relationships with Precambrian Basement*

586   *Fabric*

587   The northern segment of the Lupa Fault exhibits clear alignment with the trend of the Katuma

588   Terrane (Fig. 10) and with a few interpretable magnetic lineaments (likely due to low resolution

589   of the aeromagnetic data). We also note that the Lupa Fault is sub-parallel to the Chisi Shear

590   Zone in this area. Farther south of the Lupa Fault (Kapalala-Kanga area; Figs. 10 A-C), the fault

591   segments occur at a high angle to the Usagaran Belt and Lupa Terrane fabrics, thus indicating an

592   apparent lack of control of pre-existing basement fabric on the propagation of the southern Lupa

593   Fault, except in the coincidence of the fault steps with the trend of the basement fabrics.

594   The southern segment of the Lupa Fault transitions into the Rungwe Volcanic Province

595   (RVP) where surficial cover of volcanic deposits obscures the southward continuation of the

596   Lupa Fault (Fig. 11A). In addition, the presence of mafic volcanic deposits in the RVP (e.g.,

597   Fontijn et al., 2012) makes it difficult to make a reliable interpretation of the magnetic fabric of

598   the underlying Precambrian basement (Fig. 11B). However, we find that a distinct magnetic-high

599   lineament aligns with the Mbaka Fault surface trace (white arrows in Figs. 11A and 11B). Also,

600   the distribution of volcanic centers in the RVP show alignment with both the Mbaka Fault trace

601   and a subtle curvilinear gradient (black arrows in Fig. 11B). Further south, the curvilinear

602   gradient connects with the Livingstone Fault, the northeastern border fault of the North Malawi

603   Rift. This curvilinear gradient coincides with the location and extents of the so-called "Ngozi-

604   Rungwe Line" of Fontijn et al. (2010), described as a buried fault system that served as a conduit

605   for magmatic fluids to migrate to the surface volcanic vents. Therefore, although it is possible

606   that the magnetic anomalies in this area are affected by remanent magnetization from the

607   volcanic deposits, we interpret that this aeromagnetic gradient provides a possible subsurface

608   evidence of the fault system (Ngozi-Rungwe Line) that connects the Lupa Fault and the

609   Livingstone Fault across the RVP. The filtered aeromagnetic data and previous field studies

610   (e.g., Wheeler and Karson, 1989) shows that the Livingstone Fault segments align with and

611   reactivated the fabric of the Upangwa Terrane (Figs. 11B-C). The observations and

612   interpretations above suggest that there exists a well-developed continuous connectivity of rift-

613   related structures along the northeastern boundary of the RNMRS. However, the relationship

614   between the basement fabric and the buried faults beneath the volcanic deposits remains unclear.

615

616   *5.4. Implications for Rift Development*

617   *5.4.1. Rift Coupling*

618   In the Rukwa Rift, the substantial dominance of the Ufipa Fault rift shoulder over that of the

619   Lupa Fault may imply that the Ufipa Fault is the present-day active border fault of the Rukwa

620   Rift. This proposition may be supported by the hypocentral location of the 1994 Mw5.9 Rukwa

621   earthquake and its aftershoks with epicentral location in the northern part of the rift (Fig. 12;

622   Zhao et al., 1997). The nodal planes of the earthquake focal mechanism solution are broadly

623 consistent with the orientation of both the Lupa and Ufipa faults, and relative position of

624 aftershocks to the main shock is well determined (Fig. 12; Zhao et al., 1997). Considering the

625 uncertainty range of the earthquakes, the spatial distribution of the aftershocks relative to the

626 main shock delineates a sub-horizontal fault zone that most fits the subsurface projection of the

627 Ufipa Fault (Fig. 12). In addition, field investigations of the Kwera relay ramp (see Fig. 6 for

628 location) revealed features that indicate recent activity along the Ufipa Fault (Delvaux et al.,

629 2012). Camelbeeck and Iranga (1996) observed several lower crustal seismicity in the Rukwa

630 Rift with most of the events clustering beneath the Songwe Trough and the Rungwe Volcanic

631 Province (southern parts of the rift; Fig. 1B). The locations of the clusters suggest activity along

632 the southern Lupa Fault and Mbeya Range Fault. However, since the scarp height (and throw?)

633 of the Ufipa Fault decreases southwards (Fig. 3), and the throw on the Lupa Fault increases

634 southwards (and rapidly along the Songwe Trough) (Morley et al., 1992), we infer that the

635 present border fault role of the Ufipa Fault excludes the southernmost parts of the Rukwa Rift.

636   It has also been observed that the early stage of continental rifting is typically

637 characterized by the development of along-axis alternating polarity of rift segments, rift border

638 faults, uplifted rift flanks (e.g., Bosworth, 1985; Rosendahl, 1987; Hayward and Ebinger, 1996;

639 Lao-Davila et al., 2015). The zones of polarity changes (transfer/accommodation zones) serve to

640 transfer extensional strain between the rift segments and link the border faults which often have

641 variable structural styles and geometries (e.g., Morley et al., 1990; Wilson, 1999). Within young

642 continental rift settings, interactions between these large border faults lead to the systematic

643 coupling of border faults and rift segments across the transfer zones, and subsequent growth of

644 the rift system (e.g., Corti, 2012). Along the RNMRS, the alternating location of the of rift

645 shoulder uplift (SW in Rukwa Rift and NE in North Malawi Rift), typical of coupled rift

646   segments, suggest that the RNMRS can be considered a coupled rift segment. Further, our study

647   here shows that there is in fact, continuous structural continuation along the northeastern and

648   southwestern margins of the RNMRS, typical of a coupled rift segment. Although, studies in the

649   EARS and illustrations of its rift segments had always assumed this to be true, we hereby

650   provide evidence supporting it, for the first time. In the West Antarctic rift system, the

651   localization of recent volcanism along transverse structures within an accommodation zone (the

652   Discovery accommodation zone) suggests active structural interactions between the flanking rift

653   segments (Wilson, 1999). Therefore, we further suggest that the focusing of Neogene volcanism

654   (e.g., Fontijn et al., 2010, 2012) along the northeastern boundary faults of the Mbozi

655   accommodation zone (Fig. 15A) may be indicative of the ongoing coupling of the Rukwa and

656   North Malawi Rift's northeastern border faults.

657

658   *5.4.2. Rift Kinematics*

659   Several studies have suggested that the development of the RNMRS has been dominated by

660   dextral strike-slip kinematics (e.g., Chorowicz, 1989; Daly et al., 1989; Wheeler and Karson,

661   1994; Kervyn et al., 2006; Mortimer et al., 2007). However, analyses of fault architecture, fault-

662   kinematics, paleostress and present-day earthquake focal mechanism solution in the Rukwa Rift

663   show that the present-architecture of the rift largely developed within a pure extensional setting

664   with extension direction orthogonal to the trend of the RNMRS (Morley, 2010; Delvaux et al.,

665   2012). Furthermore, Delvaux et al. (2012) observed dextral strike-slip faulting along the fault

666   systems bounding the Rukwa Rift, but concluded that the strike-slip event was transitory and was

667   associated with an early Mesozoic transpressional event that resulted in the inversion of Karoo

668   sediments. In this study, we observe the existence of a well-defined strike-slip fault bounding the

669   SW margin of the Mbozi Block that reactivated the Precambrian Mughese Shear Zone. We also

670   observe lack of present-day activity along the strike-slip fault, and that this fault displaced a

671   buried mafic dike with at least 500 m of dextral offset.

672   In the absence of chronological data on the mapped dike, we posit that the dike is most-

673   likely associated with the widespread late-Karoo dike swarms observed in the Luangwa Rift and

674   Shire Graben (southern Malawi) (Castaing, 1991; Van de Velde and De Waele, 1998). We refer

675   to this strike-slip fault as the "Mughese Fault", and the buried dike as the "Chitipa Dike". The

676   Chitipa Dike, presented for the first time in this work, may constitute the most excellent record

677   of strike-slip kinematics along the RNMRS. Although, our results agree with Delvaux et al.

678   (2012) in that the strike-slip faulting along the RNMRS was short-lived, we suggest that future

679   geochronological analyses of this intrusion may provide the most-reliable constraint on the

680   timing of strike-slip faulting event. It is also interesting to note that if the Mughese strike-slip

681   fault is post-Karoo, its development represents a late reactivation of the Mughese Shear Zone in

682   the evolution of the RNMRS. However, late reactivation of rift-oblique basement shear zones is

683   not uncommon in rift basins (e.g., Muirhead and Kattenhorn, 2018).

684   Following the considerations above, we present cartoons of the RNMRS, illustrating the

685   continuous structural connectivity along the northeast and southwest boundaries guided by the

686   basement fabrics (Fig. 15B), and possible subsurface geometries and interactions of the domain-

687   bounding structures (Fig. 15B-E). The inferred dominance of the Ufipa Fault in the northern and

688   central parts of the Rukwa Rift (Fig. 12) suggest possible truncation of the Lupa Fault at depth,

689   such that the load of the basin hanging wall block is being carried by the Ufipa Fault (Fig. 15B).

690   However, seismic data is needed to confirm this interpretation. We illustrate a possible spatial

691   relationship between the RVP magma pathways and the Mbozi Block bounding faults in Figure

692 15C. In Figure 15D-E, we show a generalized basin geometry and flip in border fault polarity

693 from the Malawi Rift North Basin to the Usisya Basin. Overall, we posit that, along the

694 northeastern boundary of the Mbozi Block transfer zone strain is accommodated by magmatism

695 utilizing pre-existing fault systems, whereas, along the southwestern boundary, strain is

696 accommodated by dextral strike-slip faulting.

697

698 *5.5. Control of basement fabrics on normal fault geometries*

699 Overall, along the border faults of the Rukwa Rift, we find that strongly-curvilinear normal fault

700 geometries (in plan-view) occur in three distinct settings. One, in areas where the basement

701 fabrics describe high curvatures (>15°) (e.g., in the Chisi area, northern segment of the Lupa

702 Fault; Fig. 5). Second, in areas of superposition of discordant sets of basement fabrics, in which

703 the overall fault strike is parallel to one of the sets and relay ramp breach-faults follow the other

704 fabric set that is oblique to the overall fault strike (e.g., central segment of Ufipa Fault; Fig. 6).

705 Third, in areas where the faults propagate at high-angle to the strike of the basement fabrics (e.g.,

706 in the Kapalala-Kanga area, southern segment of the Lupa Fault; Fig. 10). In general, along the

707 RNMRS, we find that in areas where the basement fabrics show low curvatures (<10°), the fault

708 segments tend to describe long, rectilinear geometries with narrow or almost unidentifiable

709 breached-relay zones (e.g., Southern Ufipa Fault, Fig. 7; Mughese Fault, Fig. 8; Livingstone

710 Fault, Fig. 11). We suggest that the control of rectilinear (<10° curvature) basement fabrics on

711 the propagation of normal faults may result in the development of rectilinear fault segments with

712 greater likelihood of occurrence of narrow relay ramps and tip-to-tip fault linkage.

713 Curvilinear normal faults have been observed at various scales and at different

714 extensional tectonic settings (Fossen and Rotevatn, 2016). However, the first order curvilinear

715   normal faults are typically characterized by segment boundaries with salients (cusps) that plunge

716   basin-ward e.g., Salt-lake salient and Transverse Mountain salients of the Wasatch Fault in Utah

717   (Fig. 16A), and the Gullfaks salient in the North Sea (Fig. 16B) (Fossen and Rotevatn, 2016).

718   Also, the reported curvilinear faults show characteristic basin-ward concave geometries.

719   However, the South Oquirrh Mountains normal fault zone, although curvilinear (Wu and Bruhn,

720   1994), exhibits striking basin-ward convex geometry in which the cusps point into the footwall

721   of the fault (Fig. 16A). Wu and Bruhn (1994) suggested that convex curvilinear geometry of the

722   South Oquirrh Mountains normal fault zone developed by sequential propagation of the fault into

723   its foot-wall, guided by linkage across smaller en-echelon faults created by the lateral shear

724   components at the tips of the propagating fault. Here, in the Rukwa Rift, we observe both

725   convex- and concave-curvilinear normal fault geometries along the Ufipa and Lupa Faults. The

726   central Ufipa Fault (Fig. 6) and southern Lupa Fault (Kapalala-Mwambani area in Fig. 10A-C)

727   exhibit convex-curvilinear normal fault geometries, whereas the northern Ufipa Fault and the

728   Chisi Fault demonstrate concave-curvilinear fault geometries (linked at the Chisi salient) (Fig.

729   5). Also, we find striking similarities between the concave- and convex-curvilinear fault

730   geometries of the Rukwa Rift (Fig. 16C) with those in the southern Malawi Rift (Fig, 16D), the

731   Jurassic sedimentary sequence of the northern North Sea rift (Gullfaks area) (Fig. 16B), and the

732   Provo-Salt Lake City area (Fig. 16A). As show in Figure 16D, the segments of the Bilila-

733   Mtakataka Fault in southern Malawi Rift present excellent examples of convex-curvilinear

734   normal fault geometries (Jackson and Blekinsop, 1997). Recent studies on the relationships

735   between the basement fabrics and the Bilila-Mtakataka Fault segments (Johnson et al., 2018;

736   Hodge et al., 2018) show that some of the segments appear to align with the distributed basement

737   fabrics, while others cut across the basement fabrics.

738   Based on the observations above, we present conceptual models for the control of

739   various configurations of pre-existing basement fabrics on the development of curvilinear normal

740   fault plan-view geometries (Fig. 17). We show how discrete and distributed basement fabrics and

741   combinations of the two categories of fabrics can influence the plan-view geometry of normal

742   faults. However, there is need to better understand (1) the influence of the basement fabrics on

743   the geometries of curvilinear normal faults in 3-dimensions, (2) the influence of the extension

744   direction on the development of the observed curvilinear normal faults in areas where the

745   basement fabric present mechanical anisotropy.

746   Although, Fossen and Rotevatn (2016) provide evidence of subsidiary short-cut faulting

747   across a salient, suggesting an impending evolution of concave-curvilinear faults into rectilinear

748   faults, it is not yet clear if the model applies to convex-curvilinear normal faults since the two

749   styles of faults are geometrically different. However, the synthetic Bilila-Mtakataka and the

750   Chirobwe-Ncheu Faults (Fig. 16D) in southern Malawi Rift may provide some insight. Since the

751   Chirobwe-Ncheu Fault is older than the Bilila-Mtakataka Fault (Jackson and Blekinsop, 1997),

752   the rectilinear geometry of the Chirobwe-Ncheu Fault suggests that the apices of convex

753   curvilinear segments may likewise eventually get breached to form more-rectilinear fault

754   segments. Conversely, we observe the opposite of this model along the Lupa Fault, where the

755   more-rectilinear northern Lupa Fault has accommodated much less strain compared to its

756   curvilinear southern segment which has the most strain within the Rukwa Rift (Morley et al.,

757   1992). Therefore, we suggest that although the model of temporal progression from a curvilinear

758   to rectilinear fault geometry may apply to some large normal faults, it may not apply to others.

759

760

5.6. Rift Bifurcation

The basin scale splaying of the Rukwa Rift around the Mbozi Block into the Musangano and Songwe Troughs (Fig. 1B) obviously represents a smaller-scale of rift bifurcation when compared to the continental scale bifurcation of rift systems around microplates. Examples of such continental-scale rift bifurcation include the branching of the East African Rift around the Tanzania microplate into the western and eastern branches (Fig. 1A; e.g., Rosendahl, B.R., 1987; Versfelt and Rosendahl, 1989), the Red Sea Rift around the Sinai microplate into the Gulf of Suez Rift and Dead Sea Transform, and the South Atlantic Rift around the Sergipe microplate into the Tucano-Recôncavo Rift and Sergipe-Alagoas Transform (e.g., Szatmari and Milani, 1999) (Figs. 18A-C). Based on scale distinction, we therefore refer to the continental rift-system scale bifurcation as first (1st) order rift bifurcation (Figs. 18A-C) and the rift-basin scale bifurcation as second (2nd) order rift bifurcation (Fig. 18D-F). Similar to the Rukwa Rift, 2nd order rift bifurcations are common along the East African Rift System. Examples include the Southern Malawi Rift bifurcation around the Shire Horst, the Shire Graben bifurcation around the Namalambo Horst, and the Albertine Graben bifurcation around the Rwenzori Block (Fig. 18B; e.g., Castaing, 1991; Koehn et al., 2008; Lao-Davila et al., 2015; Xue et al., 2017).

Regardless of scale, numerical models have showed that inherited structural heterogeneity and lateral strength variations are key controls on rift bifurcation (e.g., Brune and Autin, 2013; Brune et al., 2017). However, it appears that 1st order bifurcations commonly occur at the tip of pre-existing microcratonic blocks along the path of propagation of a continental rift system (e.g., Fig. 18A). Also, 2nd order bifurcations appear to occur at the transfer zones between approaching rift segments, possibly due to a high tendency for the development of interfingering fault blocks in the transfer zones between colinear approaching rift segments (Morley, 1995) and

784 lateral rotation of the trapped blocks in the transfer zones between overlapping approaching rift

785 segments (Koehn et al., 2008).

786   It is possible that the bifurcation of the Rukwa Rift around the Mbozi Block is related to

787 the location of the block within the transfer zone of the colinear approaching Rukwa and North

788 Malawi Rift segments. However, we suggest that the basement fabrics of the Ubendian Belt

789 around the Mbozi Block transfer zone could be playing a complementary role in facilitating and

790 guiding the intra-rift bifurcation of the Rukwa Rift around the block. Our filtered aeromagnetic

791 map (Fig. 4B) shows that the block is dominated by a WNW-ESE and N-S fabrics. According to

792 Daly (1988), the Meta-basites and intermediate granulites and quartzites of the Mbozi Block are

793 characterized by lineations that trend NE-SW. These observations, however, suggest that the

794 Mbozi Block fabrics strike at oblique to high-angles to the trend of the colinear fabrics of the

795 basement terranes bounding the Mbozi Block (Katuma-Upangwa Terranes to the northeast, and

796 those of the Ufipa Terrane to the southwest) and the main rift-bounding faults (the Lupa, Ufipa,

797 Livingstone and Mughese Faults) (Fig. 15A). Therefore, we suggest that the colinear fabrics of

798 the basement terranes surrounding the Mbozi Block which are already controlling the

799 propagation and linking of the rift-bounding faults may be playing a significant role in guiding

800 the bifurcation of the Rukwa Rift around the Mbozi Block (Figs. 4B, 7, 8 and 11).

801

802 **6.0 CONCLUSIONS**

803   Our topographic analyses of the morphology of the RNMRS and detailed study of the

804 relationships between the pre-existing basement fabric and rift-related faults provide, for the first

805 time, evidence supporting the coupling of the Rukwa and North Malawi Rift. Our topographic

806 analyses in the Rukwa Rift suggest that the Ufipa Fault is the present-day active border fault of

807   the rift. We find that the Ufipa fault is the dominant topographic feature in the northern part of

808   the RMNRS and diminishes as it encounters the Mbozi block where it becomes a strike slip fault

809   (Mughese Fault), at which point the border fault polarity flips and the Livingstone Fault is the

810   dominant fault in the southern part of the RNMRS.

811   Further, we demonstrate the continuity structures along the northeastern and

812   southwestern margins of the RNMRS. We show that this structural connectivity across the

813   Mbozi Block transfer zone between the rifts is guided by the pre-existing Precambrian terrane

814   fabrics and associated shear zones. We show that the coupling of the RNMRS along the

815   northeastern boundary of the Mbozi Block transfer zone is accommodated by magmatism along

816   the linking faults, whereas, coupling along the southwestern boundary is accommodated by

817   strike-slip faulting. Overall, we suggest that the continuation of the boundary faults along the

818   RNMRS, and their alignment with colinear Precambrian basement fabric and shear zones

819   indicate the influence of the pre-existing basement structures on the coupling and amalgamation

820   of approaching colinear rift segments. On the basin-scale bifurcation of the Rukwa Rift, we infer

821   that the discordance of the basement fabrics within the Mbozi Block transfer zone to those of the

822   basement terranes bounding it may have facilitated the development of intra-rift bifurcation of

823   the rift around the transfer zone.

824   Furthermore, we show the influence of pre-existing basement fabrics on the development

825   of the RNMRS as evidenced in the geometry, termination and kinematics of the rift-bounding

826   fault segments. Our observations suggest that curvilinear normal fault geometries developed in

827   areas where the basement fabrics are either curvilinear, composed of superposed sets of

828   differently-oriented fabrics, or not favorably oriented to the extensional stress field. Whereas,

829   long, rectilinear fault geometries with narrow or almost unidentifiable breached-relay zones

830 developed in areas where the pre-existing basement fabrics are roughly rectilinear, suggesting

831 the greater likelihood of occurrence of tip-to-tip linkage of fault segments.

832 Finally, we present the existence of a buried Pre-Cenozoic strike-slip-faulted mafic dike,

833 which we suggest is potentially the most excellent record of strike-slip kinematics along the

834 RNMRS. We further suggest that future geochronological analyses of this intrusion may provide

835 the most-reliable constraint on the timing of the controversial strike-slip faulting event along the

836 RNMRS.

837

847

848   **References**

849   Baer, G., 1991. Mechanisms of dike propagation in layered rocks and in massive, porous

850   sedimentary rocks. *Journal of Geophysical Research: Solid Earth*, *96*(B7), pp.11911-

851   11929.

852   Baranov, V., 1957. A new method for interpretation of aeromagnetic maps: pseudo-gravimetric

853   anomalies. *Geophysics*, *22*(2), pp.359-382.

854   Borrego, D.J., 2016. Crustal Structure of the Rungwe Volcanic Province and Region

855   Surrounding the Northern Lake Malawi Rift Basin. MSc Thesis, Pennsylvania State

856   University.

857   Bosworth, W., 1985. Geometry of propagating continental rifts. *Nature*, *316*(6029), p.625.

858   Boven, A., Theunissen, K., Sklyarov, E., Klerkx, J., Melnikov, A., Mruma, A. and Punzalan, L.,

859   1999. Timing of exhumation of a high-pressure mafic granulite terrane of the

860   Paleoproterozoic Ubende belt (West Tanzania). *Precambrian Research, 93*(1), pp.119-

861   137.

862   Brune, S. and Autin, J., 2013. The rift to break-up evolution of the Gulf of Aden: Insights from

863   3D numerical lithospheric-scale modelling. *Tectonophysics, 607*, pp.65-79.

864   Brune, S., Corti, G. and Ranalli, G., 2017. Controls of inherited lithospheric heterogeneity on rift

865   linkage: Numerical and analog models of interaction between the Kenyan and Ethiopian

866   rifts across the Turkana depression. *Tectonics, 36*(9), pp.1767-1786.

867   Camelbeeck, T. and Iranga, M.D., 1996. Deep crustal earthquakes and active faults along the

868   Rukwa trough, eastern Africa. *Geophysical Journal International, 124*(2), pp.612-630.

869   Castaing, C., 1991. Post-Pan-African tectonic evolution of South Malawi in relation to the

870   Karroo and recent East African rift systems. *Tectonophysics, 191*(1-2), pp.55-73.

871   Chorowicz, J., 1989. Transfer and transform fault zones in continental rifts: examples in the

872   Afro-Arabian rift system. Implications of crust breaking. *Journal of African Earth*

873   *Sciences (and the Middle East), 8(2-4)*, pp.203-214.

874   Chorowicz, J., 2005. The east African rift system. *Journal of African Earth Sciences*, *43*(1),

875   pp.379-410.

876   Collanega, L., Bell, R., Coleman, A.J., Lenhart, A. and Breda, A., 2018. How do intra-basement

877   fabrics influence normal fault growth? Insights from the Taranaki Basin, offshore New

878   Zealand. EarthArxiv, DOI: 10.31223/osf.io/8rn9u

879   Corti, G., 2012. Evolution and characteristics of continental rifting: Analog modeling-inspired

880   view and comparison with examples from the East African Rift System. *Tectonophysics,*

881   *522*, pp.1-33.

882   Daly, M.C., 1988. Crustal Shear Zones in Central Africa - A kinematic approach to Proterozoic

883   Tectonics. *Episodes*, *11*(1), pp.5-11.

884   Daly, M.C., Chorowicz, J. and Fairhead, J.D., 1989. Rift basin evolution in Africa: the influence

885   of reactivated steep basement shear zones. *Geological Society, London, Special*

886   *Publications, 44*(1), pp.309-334.

887   Dawson, S.M., Laó-Dávila, D.A., Atekwana, E.A. and Abdelsalam, M.G., 2018. The influence

888   of the Precambrian Mughese Shear Zone structures on strain accommodation in the

889   northern Malawi Rift. *Tectonophysics*, *722*, pp.53-68.

890   Delvaux, D., and Hanon, M., 1991. Neotectonics of the Mbeya area, SW Tanzania. *Annual*

891   *report of the Royal Museum of Central Africa, Department of Geology and*

892   *Mineralogy*, *1992*, pp.87-97.

893   Delvaux, D., Kervyn, F., Macheyeki, A.S. and Temu, E.B., 2012. Geodynamic significance of

894   the TRM segment in the East African Rift (W-Tanzania): Active tectonics and paleostress

895   in the Ufipa plateau and Rukwa basin. *Journal of Structural Geology*, *37*, pp.161-180.

896   Delvaux, D., Levi, K., Kajara, R. and Sarota, J., 1992. Cenozoic paleostress and kinematic

897   evolution of the Rukwa–North Malawi rift valley (East African Rift System). *Bulletin des*

898   *Centres de Recherche Exploration-Production ElfAquitaine*, *16*, pp.383-406.

899   Fernandez-Alonso, M., Delvaux, D., Klerkx, J. and Theunissen, K., 2001. Structural link

900   between Tanganyika-and Rukwa-rift basins at Karema-Nkamba (Tanzania): basement

901   structural control and recent evolution. *Mus. Roy. Afr. Centr., Tervuren (Belgique), Dép.*

902   *Géol. Min., Rap. Ann*, pp.91-100.

903   Fontijn, K., Delvaux, D., Ernst, G.G., Kervyn, M., Mbede, E. and Jacobs, P., 2010. Tectonic

904   control over active volcanism at a range of scales: case of the Rungwe Volcanic

905   Province, SW Tanzania; and hazard implications. *Journal of African Earth Sciences,*

906   *58*(5), pp.764-777.

907   Fontijn, K., Williamson, D., Mbede, E. and Ernst, G.G., 2012. The Rungwe Volcanic Province,

908   Tanzania–A volcanological review. *Journal of African Earth Sciences*, *63*, pp.12-31.

909   Fossen, H., 2010. *Structural geology*. Cambridge University Press.

910   Fossen, H. and Rotevatn, A., 2016. Fault linkage and relay structures in extensional settings—A

911   review. *Earth-Science Reviews, 154*, pp.14-28.

912   Foster, A., Ebinger, C., Mbede, E. and Rex, D., 1997. Tectonic development of the northern

913   Tanzanian sector of the East African Rift System. *Journal of the Geological*

914   *Society*, *154*(4), pp.689-700.

915   Fritz, H., Abdelsalam, M., Ali, K.A., Bingen, B., Collins, A.S., Fowler, A.R., Ghebreab, W.,

916   Hauzenberger, C.A., Johnson, P.R., Kusky, T.M. and Macey, P., 2013. Orogen styles in

917   the East African Orogen: a review of the Neoproterozoic to Cambrian tectonic

918   evolution. *Journal of African Earth Sciences*, *86*, pp.65-106.

919   Gawthorpe, R.L., Jackson, C.A.L., Young, M.J., Sharp, I.R., Moustafa, A.R. and Leppard, C.W.,

920   2003. Normal fault growth, displacement localisation and the evolution of normal fault

921   populations: the Hammam Faraun fault block, Suez rift, Egypt. *Journal of Structural*

922   *Geology, 25*(6), 883-895.

923   Grauch, V.J.S. and Hudson, M.R., 2007. Guides to understanding the aeromagnetic expression of

924   faults in sedimentary basins: Lessons learned from the central Rio Grande rift, New

925   Mexico. *Geosphere*, *3*(6), pp.596-623.

926   Grauch, V.J.S. and Hudson, M.R., 2011. Aeromagnetic anomalies over faulted strata. *The*

927   *Leading Edge*, *30*(11), pp.1242-1252.

928   Gudmundsson, A. and Brenner, S.L., 2001. How hydrofractures become arrested. *Terra*

929   *Nova*, *13*(6), pp.456-462.

930   Hayward, N.J. and Ebinger, C.J., 1996. Variations in the along-axis segmentation of the Afar

931   Rift system. *Tectonics*, *15*(2), pp.244-257.

932   Helgeson, D.E. and Aydin, A., 1991. Characteristics of joint propagation across layer interfaces

933   in sedimentary rocks. *Journal of Structural Geology*, *13*(8), pp.897-911.

934   Henderson, R.G. and Zietz, I., 1949. The upward continuation of anomalies in total magnetic

935   intensity fields. *Geophysics*, *14*(4), pp. 517-534.

936   Hodge, M., Fagereng, Å., Biggs, J., and Mdala, H., 2018.. Controls on early-rift geometry: New

937   perspectives from the Bilila-Mtakataka fault, Malawi. *Geophysical Research Letters, 45*,

938   3896–3905.

939   Hodgson, I., Illsley-Kemp, F., Gallacher, R.J., Keir, D., Ebinger, C.J. and Mtelela, K., 2017.

940   Crustal structure at a young continental rift: A receiver function study from the

941   Tanganyika Rift. *Tectonics*, *36*(12), pp.2806-2822.

942   Jackson, J. and Blenkinsop, T., 1997. The Bilila-Mtakataka fault in Malaŵi: An active, 100-km

943   long, normal fault segment in thick seismogenic crust. *Tectonics*, *16*(1), pp.137-150.

944   Johnson, S., Mendez, K., Beresh, S.C.M., Mynatt, W.G., Elifritz, E.A., Laó-Dávila, D.A.,

945   Atekwana, E.A., Abdelsalam, M.G., Chindandali, P.R.N., Chisenga, C. and Gondwe, S.,

946   2017.. The Relationships of Subparallel Synthetic Faults and Pre-existing Structures in

947   the Central Malawi Rift. *AGU Fall Meeting poster number T22C-03*.

948   Katumwehe, A.B., Abdelsalam, M.G. and Atekwana, E.A., 2015. The role of pre-existing

949   Precambrian structures in rift evolution: The Albertine and Rhino grabens,

950   Uganda. *Tectonophysics*, *646*, pp.117-129.

951   Kervyn, F., Ayub, S., Kajara, R., Kanza, E. and Temu, B., 2006. Evidence of recent faulting in

952   the Rukwa rift (West Tanzania) based on radar interferometric DEMs. *Journal of African*

953   *Earth Sciences*, *44*(2), pp.151-168.

954   Kilembe, E.A. and Rosendahl, B.R., 1992. Structure and stratigraphy of the Rukwa

955   rift. *Tectonophysics*, *209*(1-4), pp.143-158.

956   Kim, S., Nyblade, A.A. and Baag, C.E., 2009. Crustal velocity structure of the Rukwa Rift in the

957   western branch of the East African Rift system. *South African Journal of Geology*, *112*(3-

958   4), pp.251-260.

959   Kinabo, B.D., Atekwana, E.A., Hogan, J.P., Modisi, M.P., Wheaton, D.D. and Kampunzu, A.B.,

960   2007. Early structural development of the Okavango rift zone, NW Botswana. *Journal of*

961   *African Earth Sciences*, *48*(2), pp.125-136.

962   Kinabo, B.D., Hogan, J.P., Atekwana, E.A., Abdelsalam, M.G. and Modisi, M.P., 2008. Fault

963   growth and propagation during incipient continental rifting: Insights from a combined

964   aeromagnetic and Shuttle Radar Topography Mission digital elevation model

965   investigation of the Okavango Rift Zone, northwest Botswana. *Tectonics*, *27*(3).

966   Koehn, D., Aanyu, K., Haines, S. and Sachau, T., 2008. Rift nucleation, rift propagation and the

967   creation of basement micro-plates within active rifts. *Tectonophysics, 458*(1-4), pp.105-

968   116.

969   Kolawole, F., Atekwana, E.A., Laó-Dávila, D.A., Abdelsalam, M.G., Chindandali, P.R., Salima,

970   J. and Kalindekafe, L., 2018. Active deformation of Malawi Rift's North Basin hinge

971   zone modulated by reactivation of pre-existing Precambrian shear zone fabric. *Tectonics,*

972   *37*, pp.683–704.

973   Lao-Davila, D.A., Al-Salmi, H.S., Abdelsalam, M.G. and Atekwana, E.A., 2015. Hierarchical

974   segmentation of the Malawi Rift: The influence of inherited lithospheric heterogeneity

975   and kinematics in the evolution of continental rifts. *Tectonics*, *34*(12), pp.2399-2417.

976   Lawley, C.J., Selby, D., Condon, D.J., Horstwood, M., Millar, I., Crowley, Q. and Imber, J.,

977   2013. Lithogeochemistry, geochronology and geodynamic setting of the Lupa Terrane,

978   Tanzania: implications for the extent of the Archean Tanzanian Craton. *Precambrian*

979   *Research, 231*, pp.174-193.

980   Lenoir, J.L., Liégeois, J.P., Theunissen, K. and Klerkx, J., 1994. The Palaeoproterozoic

981   Ubendian shear belt in Tanzania: geochronology and structure. *Journal of African Earth*

982   *Sciences*, *19*(3), pp.169-184.

983   Mbede, E.I., 2002. Interpretation of refelction seismic data from the Usangu Basin, East African

984   Rift System. *Tanzania Journal of Science, 28*(1), pp.83-97.

985   McCalpin, J.P., Rockwell, T.K. and Weldon II, R.J., 2009. Paleoseismology of Strike-Slip

986   Tectonic Environments. *International Geophysics, 95*, pp.421-496.

987   Modisi, M.P., Atekwana, E.A., Kampunzu, A.B. and Ngwisanyi, T.H., 2000. Rift kinematics

988   during the incipient stages of continental extension: Evidence from the nascent Okavango

989   rift basin, northwest Botswana. *Geology, 28*(10), pp.939-942.

990   Morley, C.K., 1995. Developments in the structural geology of rifts over the last decade and their

991   impact on hydrocarbon exploration. *Geological Society, London, Special*

992   *Publications*, *80*(1), pp.1-32.

993   Morley, C.K., 2010. Stress re-orientation along zones of weak fabrics in rifts: An explanation

994   for pure extension in 'oblique' rift segments?. *Earth and Planetary Science*

995   *Letters*, *297*(3), pp.667-673.

996   Morley, C.K., Cunningham, S.M., Harper, R.M. and Wescott, W.A., 1992. Geology and

997   geophysics of the Rukwa rift, East Africa. *Tectonics, 11*(1), pp.69-81.

998   Morley, C.K., Nelson, R.A., Patton, T.L. and Munn, S.G., 1990. Transfer zones in the East

999   African rift system and their relevance to hydrocarbon exploration in rifts (1). *AAPG*

1000   *Bulletin, 74*(8), pp.1234-1253.

1001 Mortimer, E., Paton, D.A., Scholz, C.A., Strecker, M.R. and Blisniuk, P., 2007. Orthogonal to

1002   oblique rifting: effect of rift basin orientation in the evolution of the North basin, Malawi

1003   Rift, East Africa. *Basin Research*, *19*(3), pp.393-407.

1004 Muirhead, J.D. and Kattenhorn, S.A., 2018. Activation of preexisting transverse structures in an

1005   evolving magmatic rift in East Africa. *Journal of Structural Geology, 106*, pp.1-18.

1006 Njinju, E.A., Atekwana, E.A., Stamps, D.S., Abdelsalam, M.G., Atekwana, E.A., Mickus, K.L.,

1007   Kolawole, F. and Nyalugwe, V., 2018. Lithospheric Structure of the Malawi Rift:

1008   Implications for Rifting Processes in Magma Poor Rift Systems. *EarthArXiv*, DOI:

1009   10.31223/osf.io/83qd9

1010 Peirce, J.W. and Lipkov, L., 1988. Structural interpretation of the Rukwa rift, Tanzania.

1011   *Geophysics, 53*(6), pp.824-836.

1012 Phillips, T.B., Jackson, C.A., Bell, R.E., Duffy, O.B. and Fossen, H., 2016. Reactivation of

1013   intrabasement structures during rifting: A case study from offshore southern

1014   Norway. *Journal of Structural Geology*, *91*, pp.54-73.

1015 Pik, R., Marty, B., Carignan, J., Yirgu, G. and Ayalew, T., 2008. Timing of East African Rift

1016   development in southern Ethiopia: Implication for mantle plume activity and evolution of

1017   topography. *Geology, 36*(2), pp.167-170.

1018 Ring, U., Kröner, A., Buchwaldt, R., Toulkeridis, T. and Layer, P.W., 2002. Shear-zone patterns

1019   and eclogite-facies metamorphism in the Mozambique belt of northern Malawi, east-

1020   central Africa: implications for the assembly of Gondwana. *Precambrian*

1021   *Research*, *116*(1), pp.19-56.

1022 Rosendahl, B.R., 1987. Architecture of continental rifts with special reference to East

1023   Africa. *Annual Review of Earth and Planetary Sciences*, *15*(1), pp.445-503.

1024   Rotevatn, A., Jackson, C.A.L., Tvedt, A.B.M., Bell, R. and Blækkan, I., 2018. How do normal

1025   faults grow?. EarthArXiv.

1026   Salem, A., Williams, S., Fairhead, J.D., Ravat, D. and Smith, R., 2007. Tilt-depth method: A

1027   simple depth estimation method using first-order magnetic derivatives. *The Leading*

1028   *Edge*, *26*(12), pp.1502-1505.

1029   Sarafian, E., Evans, R.L., Abdelsalam, M.G., Atekwana, E., Elsenbeck, J., Jones, A.G. and

1030   Chikambwe, E., 2018. Imaging Precambrian lithospheric structure in Zambia using

1031   electromagnetic methods. *Gondwana Research*, *54*, pp.38-49.

1032   Schenk, V., Boniface, N., Loose, D., Alkmim, F.F. and Noce, C.M., 2006. Paleoproterozoic

1033   subduction zones at the margins of the Tanzania and Congo Cratons: evidence from

1034   eclogites with MORB-type chemistry in the Usagaran–Ubendian Belts of Tanzania and

1035   the Nyong complex of Cameroon. *The Paleoproterozoic Record of the São Francisco*

1036   *Craton*, pp.102-103.

1037   Scholz, C.H. and Contreras, J.C., 1998. Mechanics of continental rift

1038   architecture. *Geology*, *26*(11), pp.967-970.

1039   Silva, J.B., 1986. Reduction to the pole as an inverse problem and its application to low-latitude

1040   anomalies. *Geophysics*, *51*(2), pp.369-382.

1041   Siuda, K., Magee, C., Bell, R., Jackson, C.A.L. and Collanega, L., 2018. Pre-existing basement

1042   thrusts influence rifting in the Taranaki Basin, New Zealand. EarthArXiv.

1043   Szatmari, P. and Milani, E.J., 1999. Microplate rotation in northeast Brazil during South Atlantic

1044   rifting: Analogies with the Sinai microplate. *Geology, 27*(12), pp.1115-1118.

1045   Taylor, B., Weiss, J.R., Goodliffe, A.M., Sachpazi, M., Laigle, M. and Hirn, A., 2011. The

1046   structures, stratigraphy and evolution of the Gulf of Corinth rift, Greece. *Geophysical*

1047   *Journal International, 185*(3), pp.1189-1219.

1048   Theunissen, K., Klerkx, J., Melnikov, A. and Mruma, A., 1996. Mechanisms of inheritance of

1049   rift faulting in the western branch of the East African Rift, Tanzania. *Tectonics, 15*(4),

1050   pp.776-790.

1051   Van de Velde, P., and De Waele, B., 1998. Geology of the Mupamadzi River area. Explanation

1052   of degree sheet 1231, SW quarter, Report No. 105, *Geological Survey Department,*

1053   *Republic of Zambia.*

1054   Versfelt, J. and Rosendahl, B.R., 1989. Relationships between pre-rift structure and rift

1055   architecture in Lakes Tanganyika and Malawi, East Africa. *Nature, 337*(6205), p.354.

1056   Wheeler, W.H. and Karson, J.A., 1989. Structure and kinematics of the Livingstone Mountains

1057   border fault zone, Nyasa (Malawi) Rift, southwestern Tanzania. *Journal of African Earth*

1058   *Sciences (and the Middle East)*, *8*(2-4), pp.393-413.

1059   Wheeler, W.H. and Karson, J.A., 1994. Extension and subsidence adjacent to a "weak"

1060   continental transform: An example from the Rukwa rift, East Africa. *Geology*, *22*(7),

1061   pp.625-628.

1062   Wichura, H., Bousquet, R., Oberhänsli, R., Strecker, M.R. and Trauth, M.H., 2011. The Mid-

1063   Miocene East African Plateau: a pre-rift topographic model inferred from the

1064   emplacement of the phonolitic Yatta lava flow, Kenya. *Geological Society, London,*

1065   *Special Publications, 357*(1), pp.285-300.

1066   Wilson, T.J., 1999. Cenozoic structural segmentation of the Transantarctic Mountains rift flank

1067   in southern Victoria Land. *Global and Planetary Change*, *23*(1-4), pp.105-127.

1068   Wu, D. and Bruhn, R.L., 1994. Geometry and kinematics of active normal faults, South Oquirrh

1069   Mountains, Utah: implication for fault growth. *Journal of Structural Geology*, *16*(8),

1070   pp.1061-1075.

1071   Xue, L., Gani, N.D. and Abdelsalam, M.G., 2017. Geomorphologic proxies for bedrock rivers:

1072   A case study from the Rwenzori Mountains, East African Rift system. *Geomorphology,*

1073   *285*, pp.374-398.

1074   Zhang, X. and Jeffrey, R.G., 2008. Reinitiation or termination of fluid-driven fractures at

1075   frictional bedding interfaces. *Journal of Geophysical Research: Solid Earth, 113*(B8).

1076   Zhang, X., Jeffrey, R.G. and Thiercelin, M., 2007. Deflection and propagation of fluid-driven

1077   fractures at frictional bedding interfaces: a numerical investigation. *Journal of Structural*

1078   *Geology*, *29*(3), pp.396-410.

1079   Zhao, M., Langston, C.A., Nyblade, A.A. and Owens, T.J., 1997. Lower-crustal rifting in the

1080   Rukwa graben, East Africa. *Geophysical Journal International, 129*(2), pp.412-420.

1081

1082

1083

1084

1085

1086

1087

1088

1089

1090

1091

1092
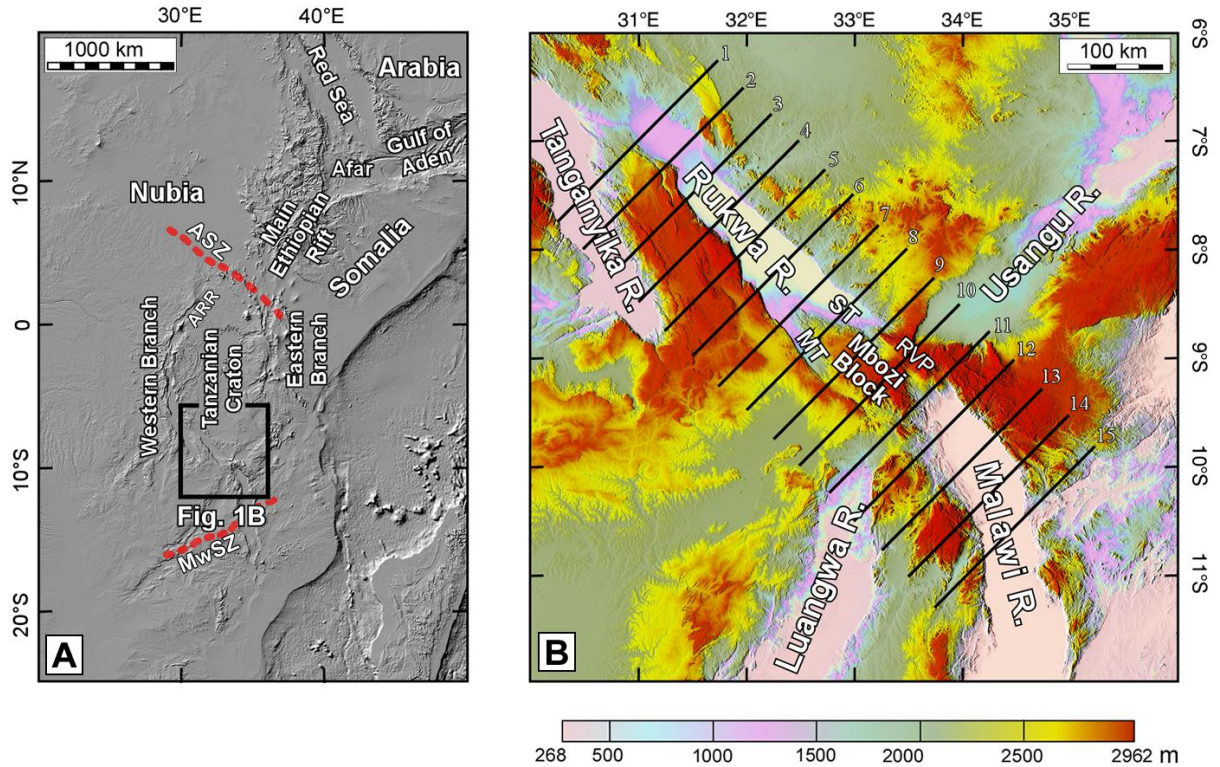
Fig.1. (A) Topographic map of the East African Rift System, showing the segments of the rift system and the location of the Rukwa-North Malawi Rift Segment (RNMRS) (black square). (B) Digital Elevation Model (DEM) of the RNMRS showing the different domains. Solid black lines represent topographic profile lines shown in Figure 3. ARR= Albertine-Rhino Rift, ASZ= Aswa Shear Zone, MT= Musangano Trough, MwSZ= Mwembeshi Shear Zone, RVP= Rungwe Volcanic Province, ST= Songwe Trough.
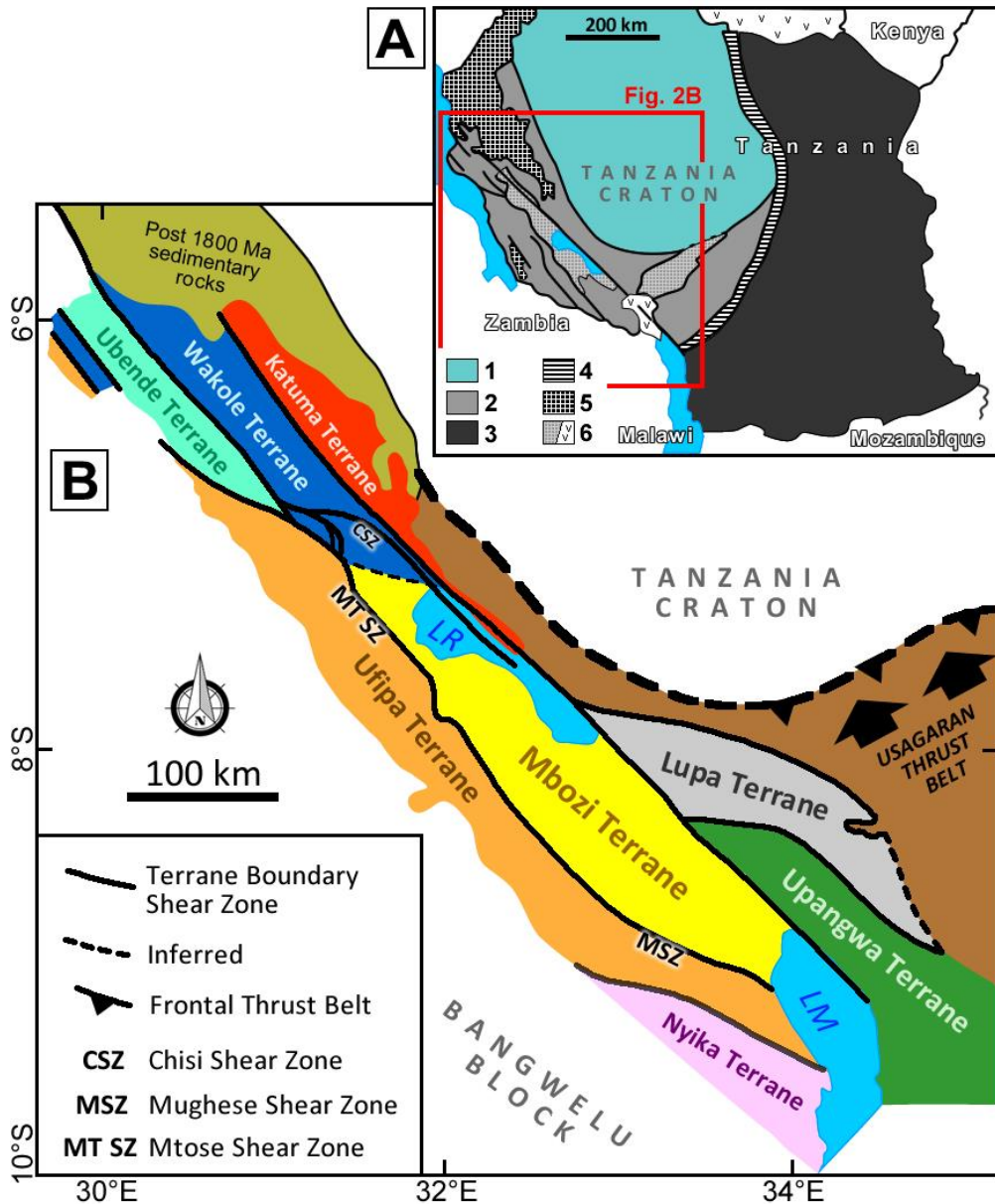
Fig. 2. (A) Precambrian domains around the Tanzanian Craton (modified after Theunissen et al., 1996; Boven et al., 1999; Fernandez-Alonso et al., 2001; Schenk et al., 2006). 1 = Archean craton; 2 = Paleoproterozoic Usagaran and Ubendian orogenic belts; 3 = Mozambique orogenic belt; 4 = western limit of Pan-African influence; 5 = Meso and/or Neoproterozoic sediments *(only for the Ubendian Belt region)*; 6 = Phanerozoic volcanics and sedimentary rocks. (B) Regional geological map of southwest Tanzania showing the terrane structure of the Ubendian orogenic belt within which the Rukwa-Malawi Rift Segment (RNMRS) developed.

49

1154

1155

1156

1157

1158

1159

1160

1161

1162

1163

1164

1165

1166

1167

1168

1169

1170

1171

1172

1173

1174

1175

1176
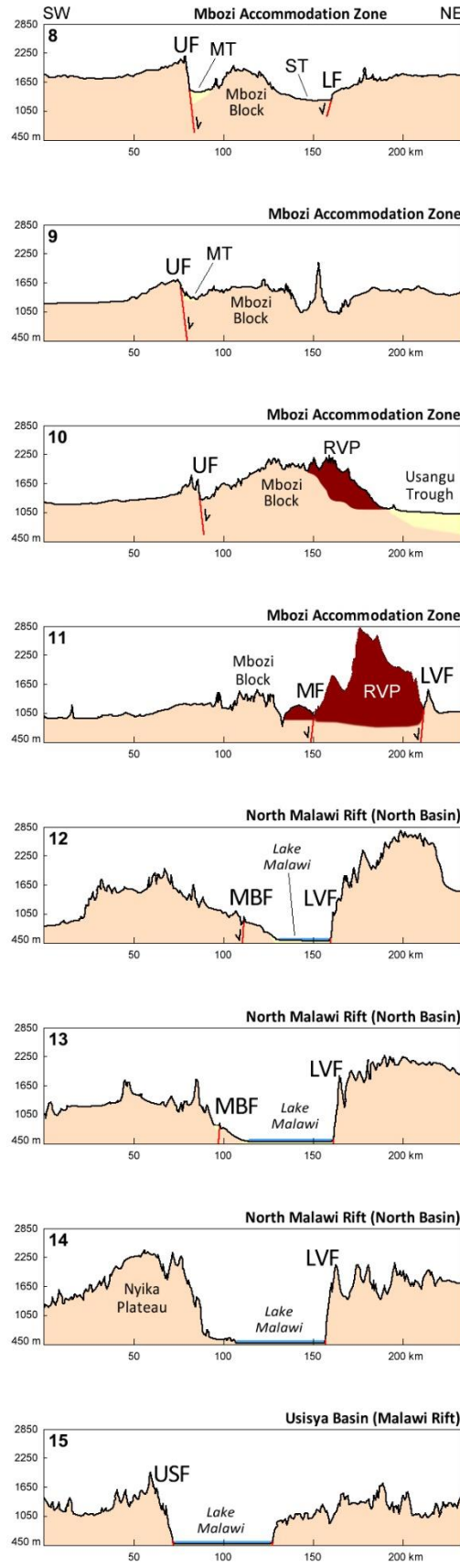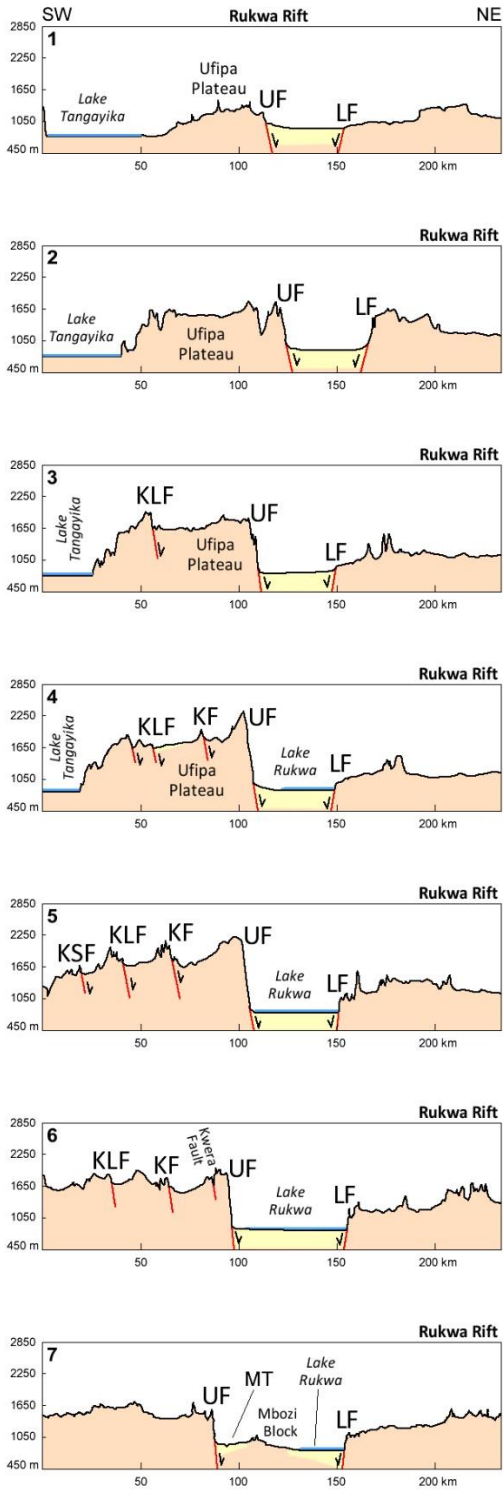
Fig. 3. Topographic profiles across the Rukwa - North Malawi Rift segment. Profile numbers correspond to the profiles in Figure 1B. KLF = Kalambo Fault, KF = Kanda Fault, KSF = Kasanga Fault, LF = Lupa Fault, LVF = Livingstone Fault, MB = Mbozi Block, MBF = Mbiri Fault, MF = Mbaka Fault, MT = Musangano Trough, RVP = Rungwe Volcanic Province, ST = Songwe Trough, UF = Ufipa Fault, USF = Usisya Fault.
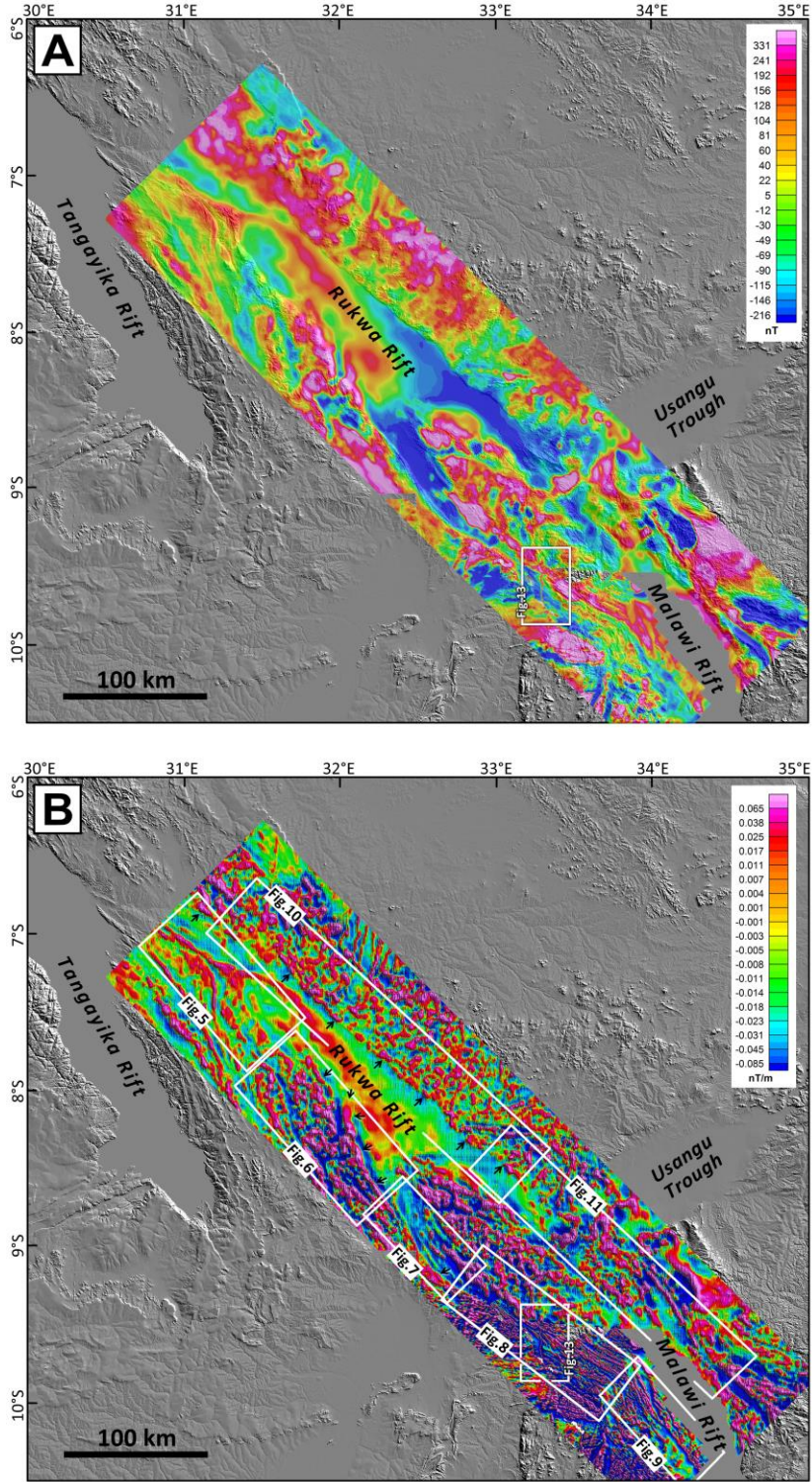
Fig. 4. (A) The reduced to pole Total Magnetic Intensity (RTP-TMI) map of the Rukwa-North Malawi Rift area, draped over the topographic digital elevation model of SW Tanzania. (B) The 1st vertical derivative map of the RTP-TMI map of the Rukwa-North Malawi Rift area draped over the topographic digital elevation model.
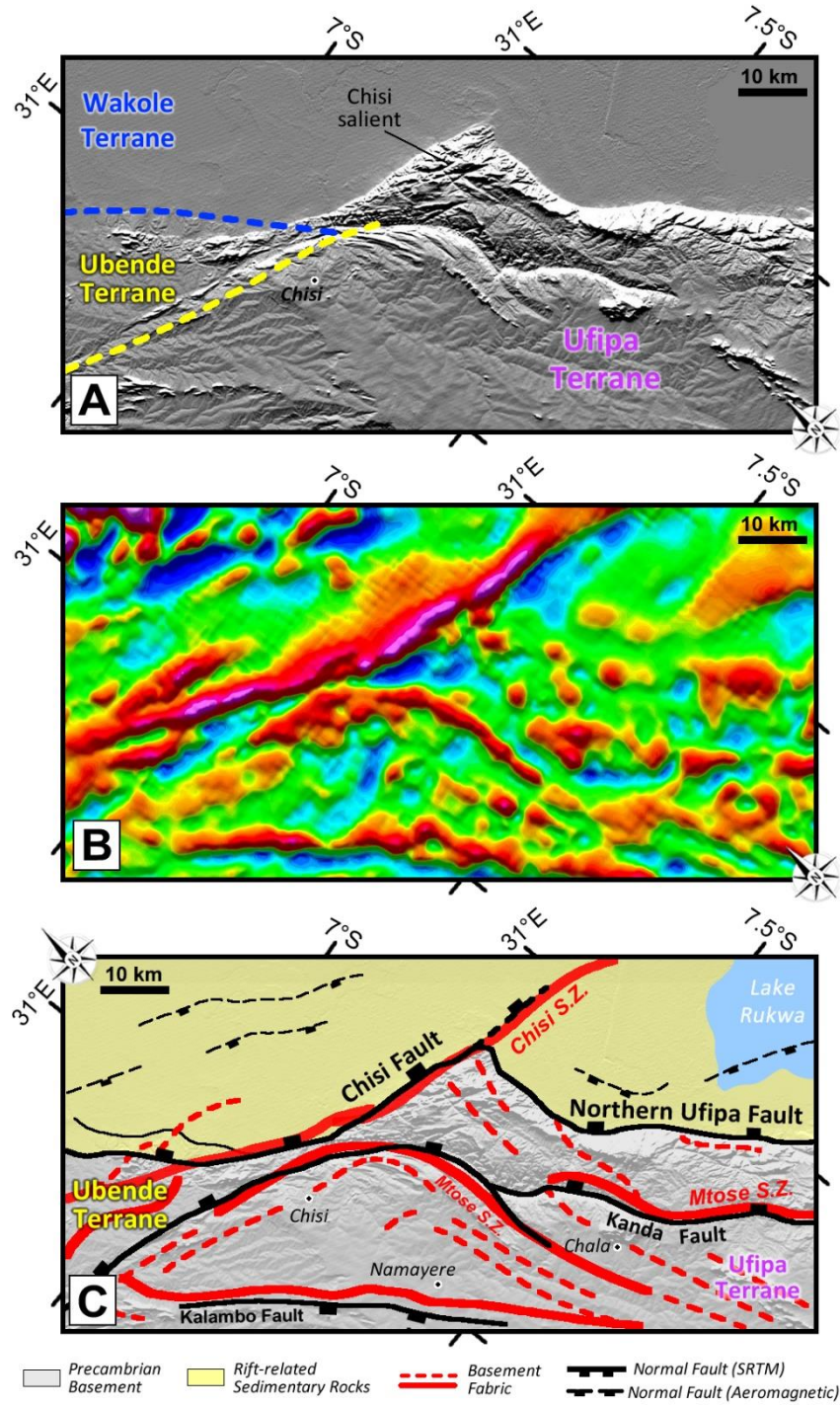
Fig. 5. Northernmost part of the Ufipa Fault, the SW boundary fault of the Rukwa Rift. Topographic digital elevation model in the top panel (A), the vertical derivative of the magnetic data in the middle panel (B), and a structural interpretation in the bottom panel (C).

53

1286
1287
1288
1289
1290
1291
1292
1293
1294
1295
1296
1297
1298
1299
1300
1301
1302
1303
1304
1305
1306
1307
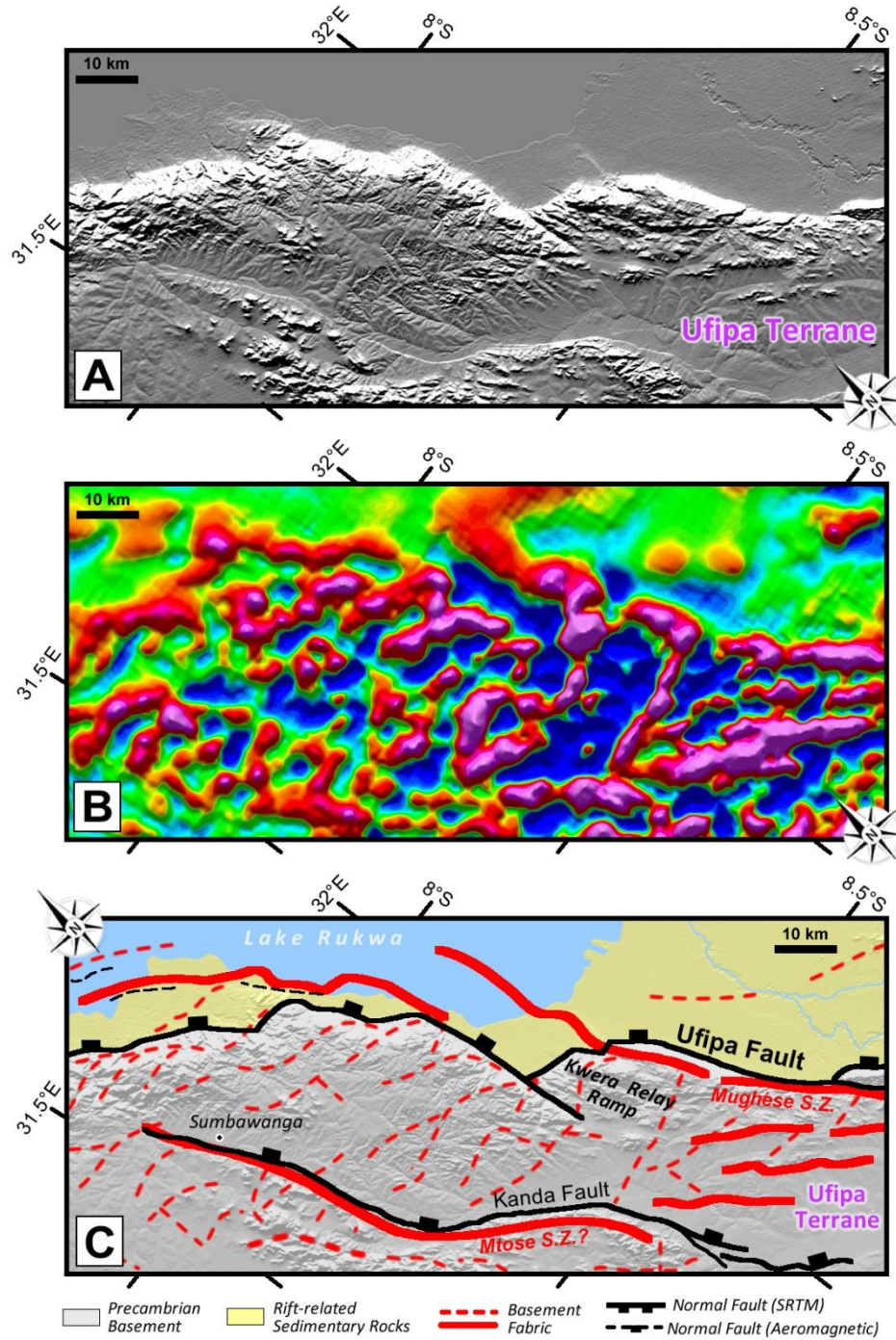
1308 Fig. 6. Central segment of the Ufipa Fault, SW boundary of the Rukwa Rift. Topographic
1309 digital elevation model in the top panel (A), the vertical derivative of the magnetic data in
1310 the middle panel (B), and a structural interpretation in the bottom panel (C).

1311
1312
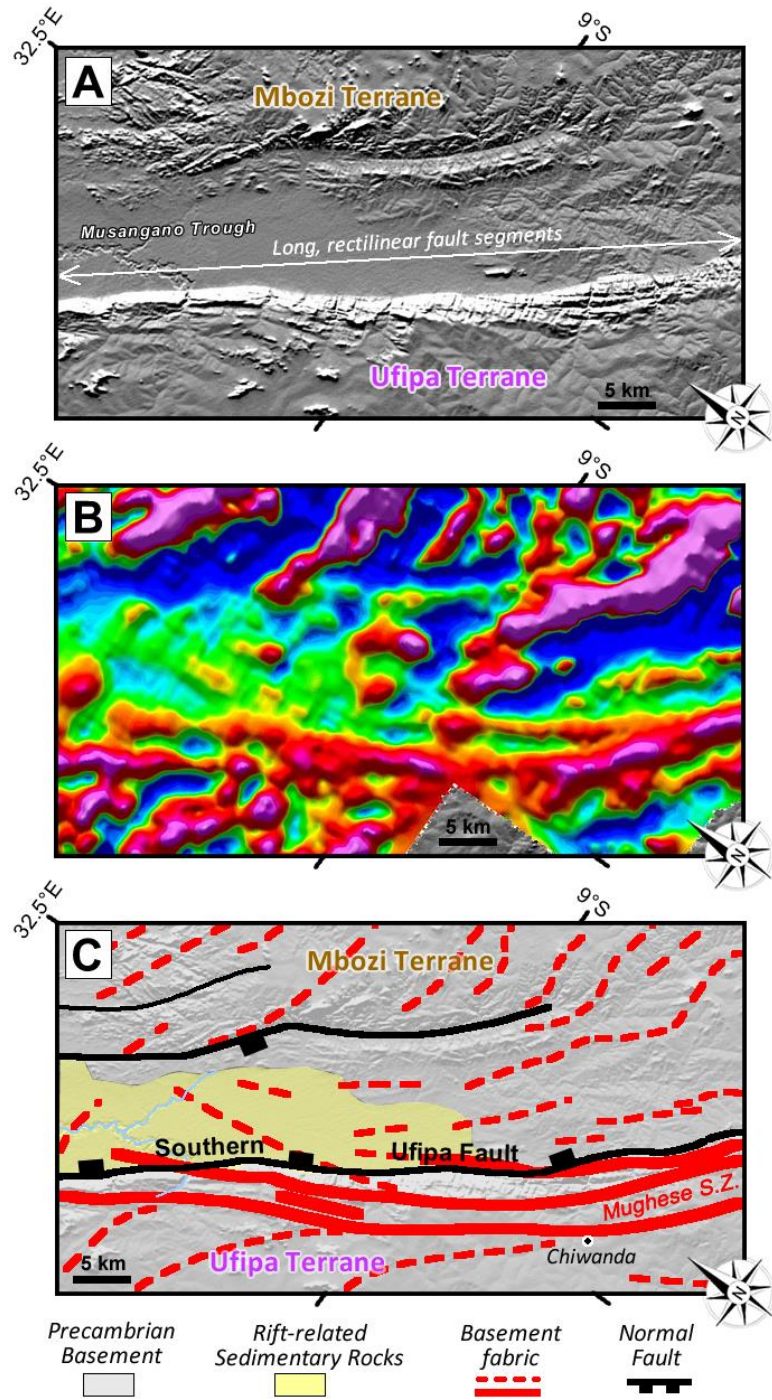
Fig. 7. The Musangano Trough part of the SW boundary of the Rukwa Rift. Topographic digital elevation model in the top panel (A), the vertical derivative of the magnetic data in the middle panel (B), and a structural interpretation in the bottom panel (C).
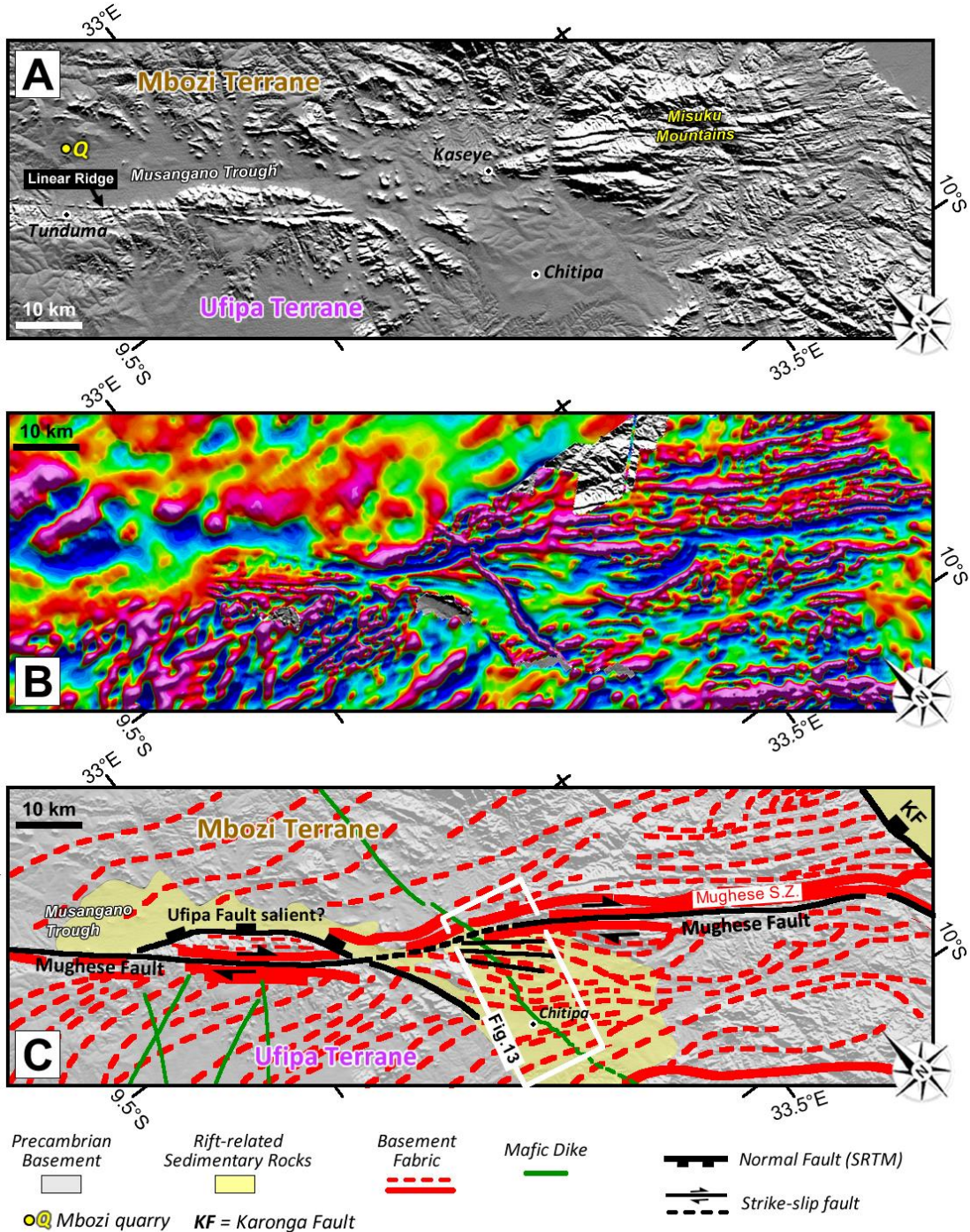
Fig. 8. The SW margin of the Mbozi Block. Topographic digital elevation model in the top panel (A), the vertical derivative of the magnetic data in the middle panel (B), and a structural interpretation in the bottom panel (C).
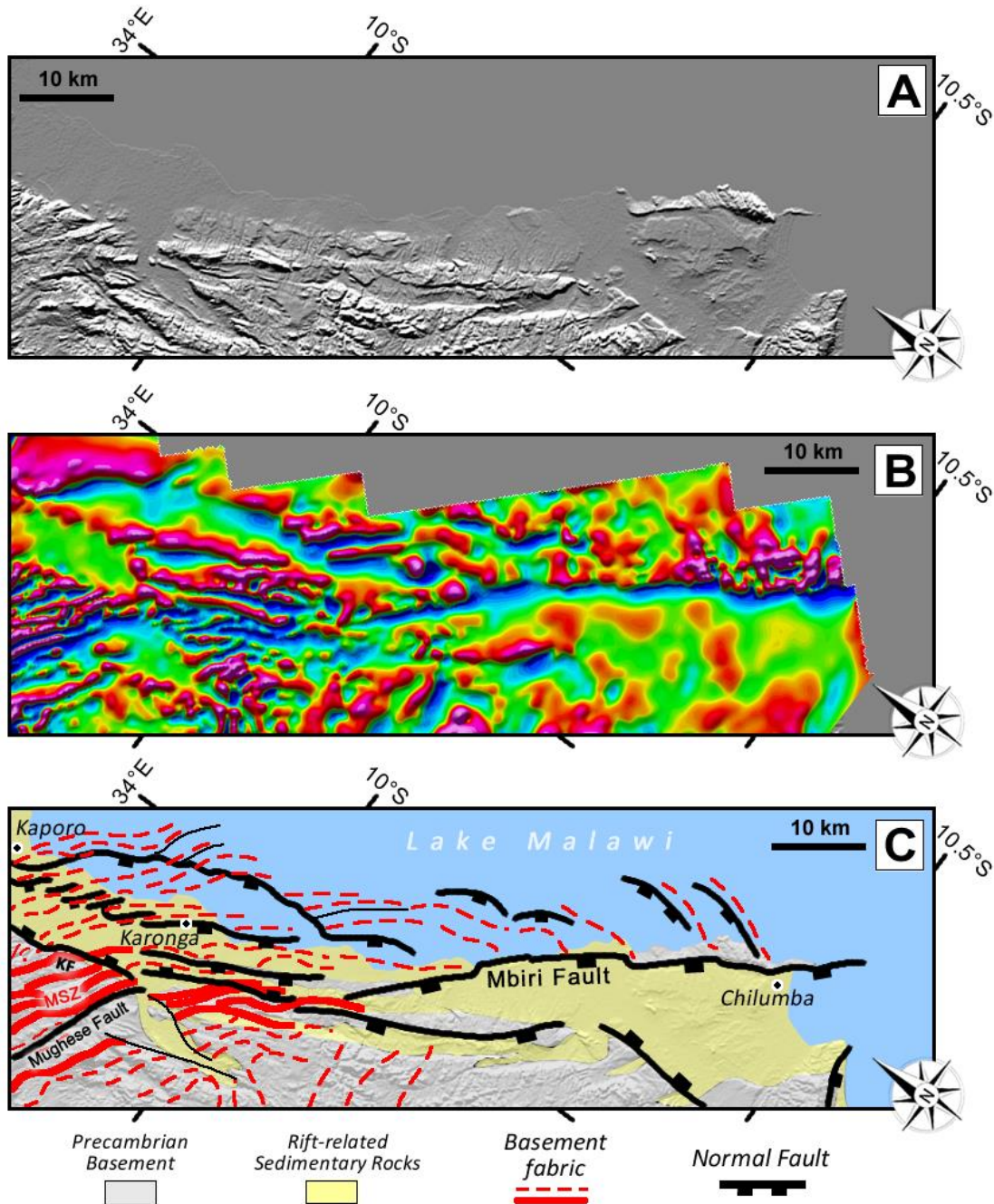
Fig. 9. The SW margin of the North Malawi Rift Basin (Karonga area). Topographic digital elevation model in the top panel (A), the vertical derivative of the magnetic data in the middle panel (B), and a structural interpretation in the bottom panel (C). MSZ = Mughese Shear Zone, KF = Karonga Fault. Fault and basement fabric interpretations from Kolawole et al. (2018).
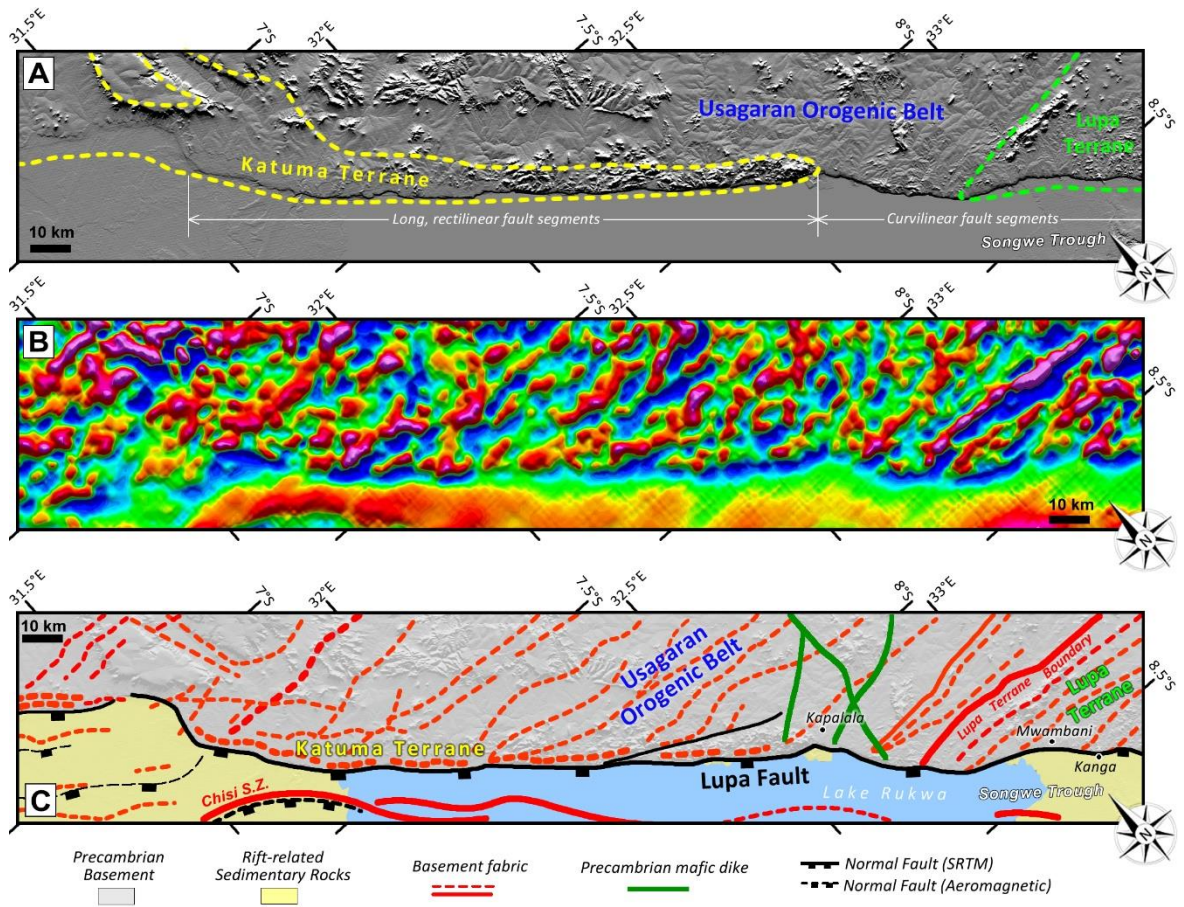
Fig. 10. The northern section of the Lupa Fault, the NE boundary fault of the Rukwa Rift. Topographic digital elevation model in the top panel (A), the vertical derivative of the magnetic data in the middle panel (B), and a structural interpretation in the bottom panel (C).

58
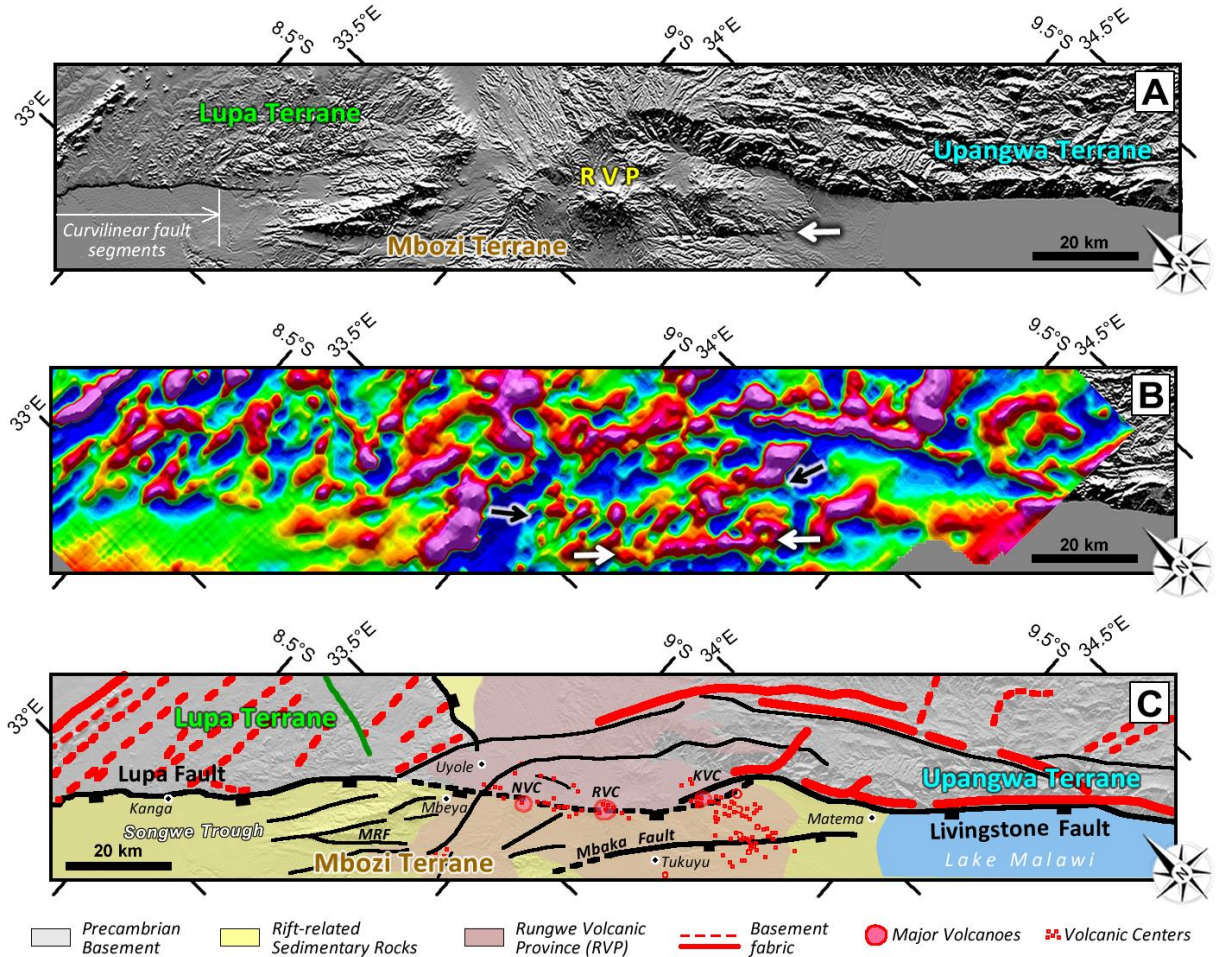
Fig. 11. The southern section of the Lupa Fault, the NE margin of the Mbozi Block (Rungwe Volcanic Province) and a section of the Livingstone Fault (NE border fault if the North Malawi Rift. Topographic digital elevation model in the top panel (A), the vertical derivative of the magnetic data in the middle panel (B), and a structural interpretation in the bottom panel (C). KVC = Kyejo Volcanic Center; NVC = Ngozi Volcanic Center; RVC = Rungwe Volcanic Center. Volcanic centers from Fontijn et al. (2010, 2012).
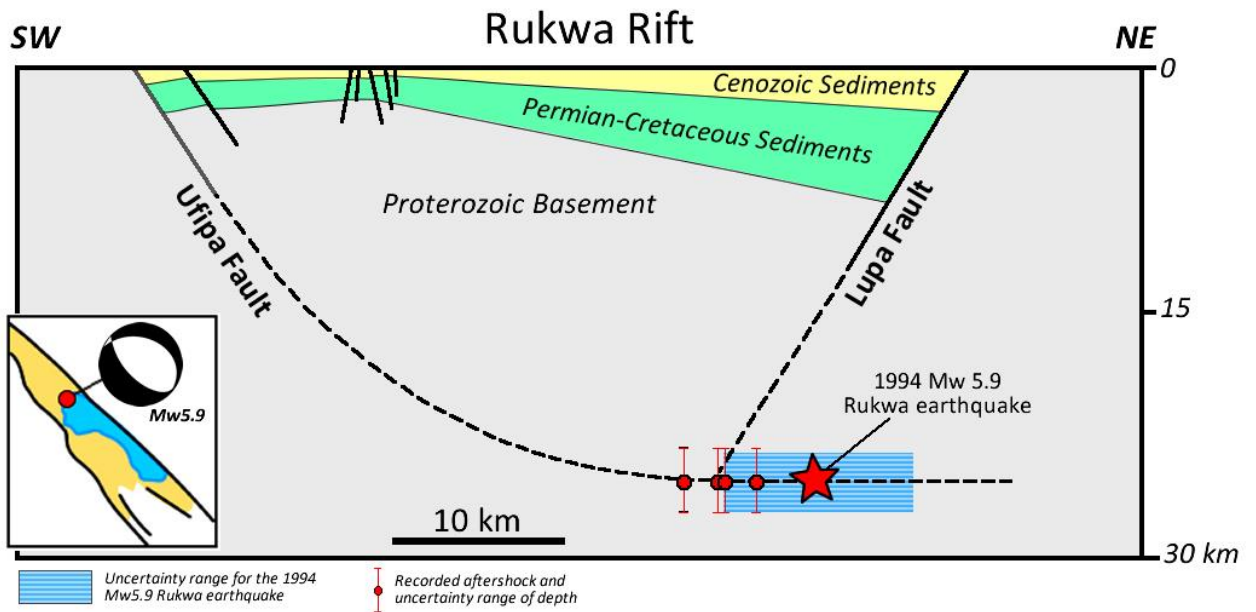
Fig. 12. Generalized geometrical relations of stratigraphic units and normal faults of the Rukwa rift, showing thickening of Cenozoic sediments towards both the Lupa and Ufipa border faults (modified after Zhao et al., 1997).
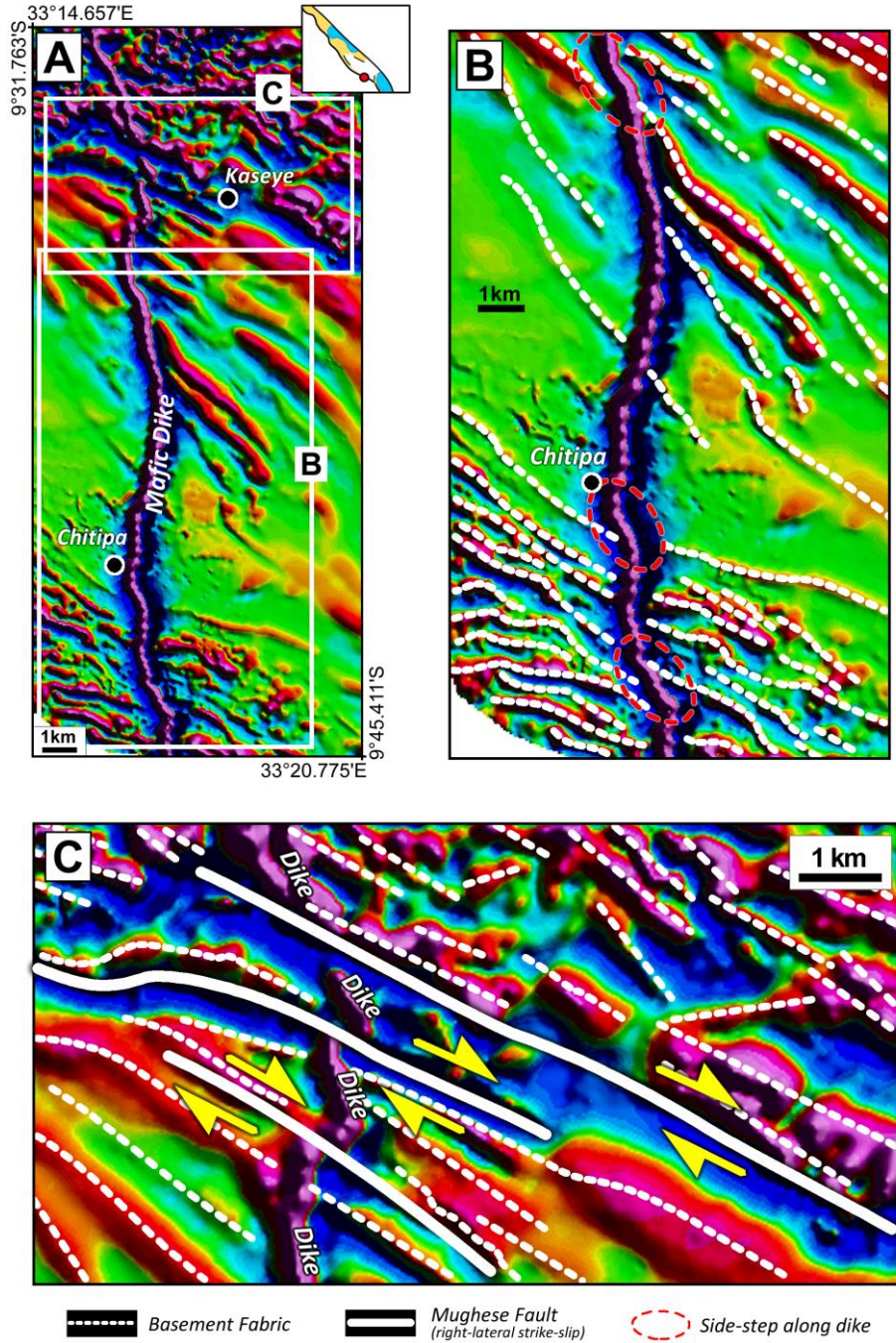
Fig. 13. (A) 1st vertical derivative of the aeromagnetic data covering the Kaseye-Chitipa area along the SW margin of the Mbozi Block (see location in top-right inset map, Figures 4A-B and 8C). (B) Close-up of the central and southern segments of a buried mafic dike (the "Chitipa Dike") showing side-stepping segments that coincide with pre-existing basement fabric. (C) Close-up of the northern segment of the dike showing right-lateral offsets by the continuation of the Ufipa Fault. This strike-slip fault segment is here-in referred to as the Mughese Fault.

1619
1620
1621
1622
1623
1624
1625
1626
1627
1628
1629
1630
1631
1632
1633
1634
1635
1636
1637
1638
1639
1640
1641
1642
1643
1644
1645
1646
1647
1648
1649
1650
1651
1652
1653
1654
1655
1656
1657
1658
1659
1660
1661
1662
1663
1664
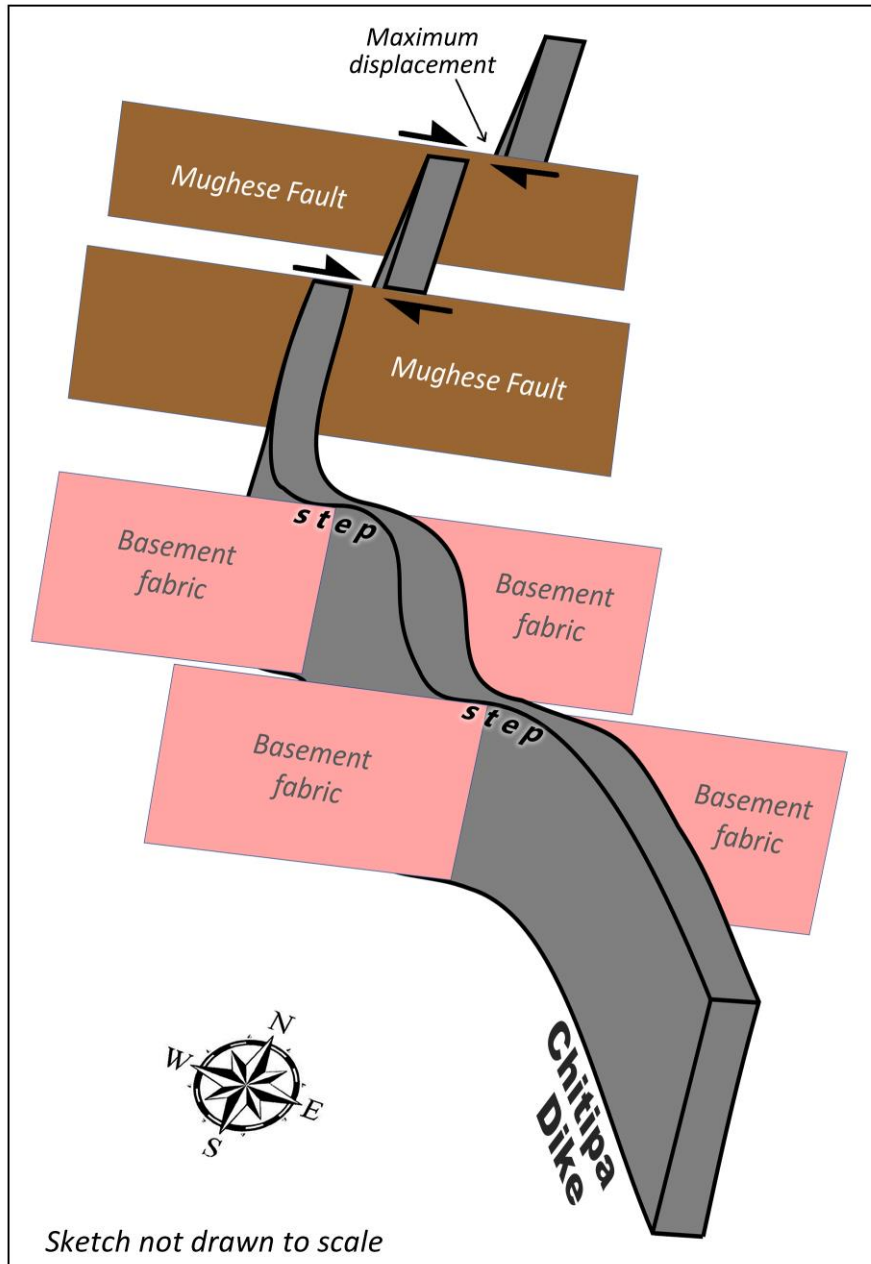
Fig. 14. 3-dimensional (3-D) conceptual model of the geometry of the interpreted dike (the "Chitipa Dike") and its interactions with the pre-existing basement fabric and the post-emplacement Mughese strike-slip fault offset.
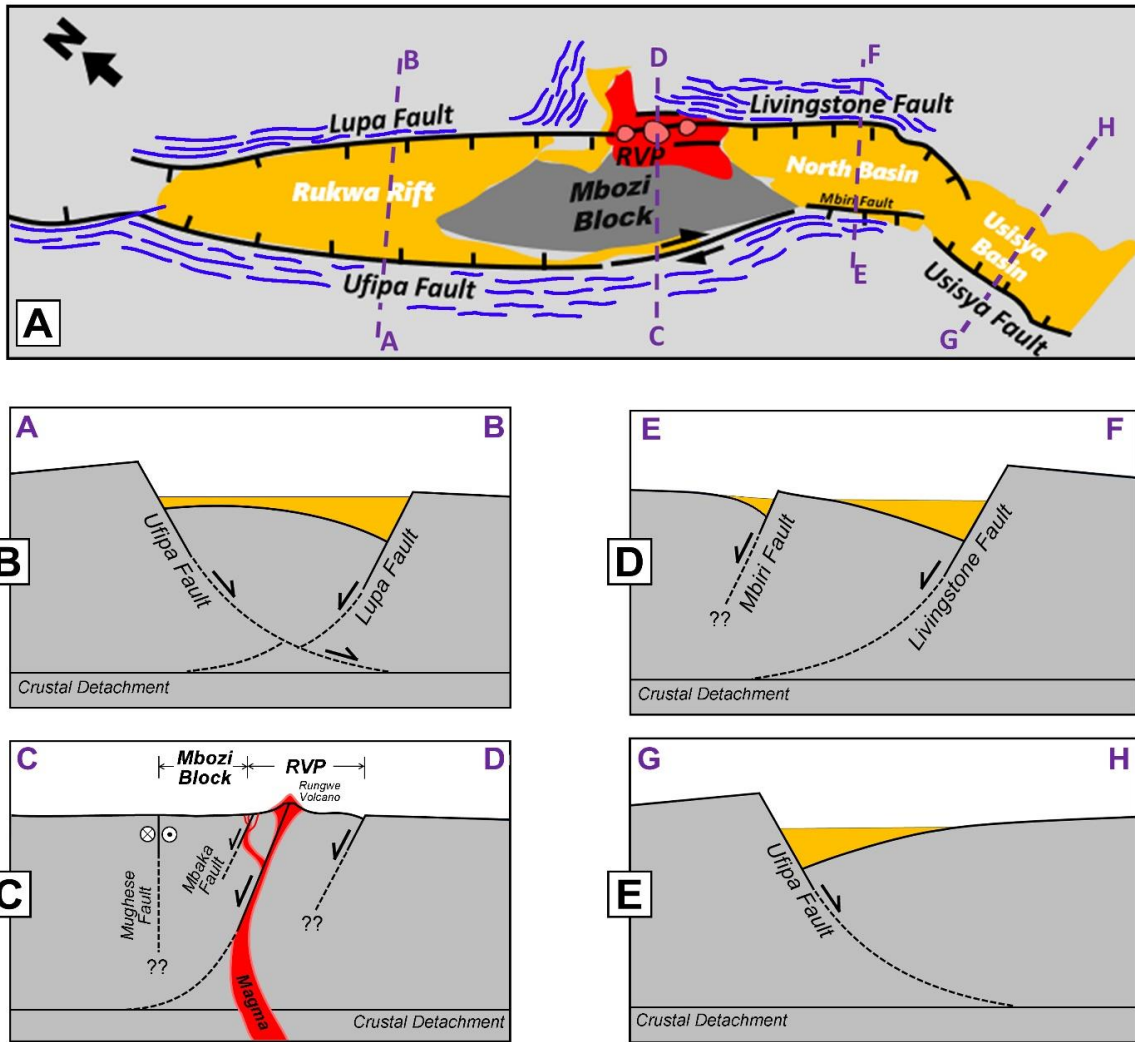
Fig. 15. (A) Generalized cartoon (map view) of the Rukwa-North Malawi Rift Segment (RNMRS) illustrating the continuous structural connectivity along the northeast and southwest boundaries, guided by the basement fabric. Black solid line = fault, blue solid line = basement fabric. RVP = Rungwe Volcanic Province. (B-E) Cross-section cartoons across the segments of the RNMRS, illustrating the possible subsurface geometries and interactions of the domain-bounding structures. LLF = Livingstone-Lupa Fault.
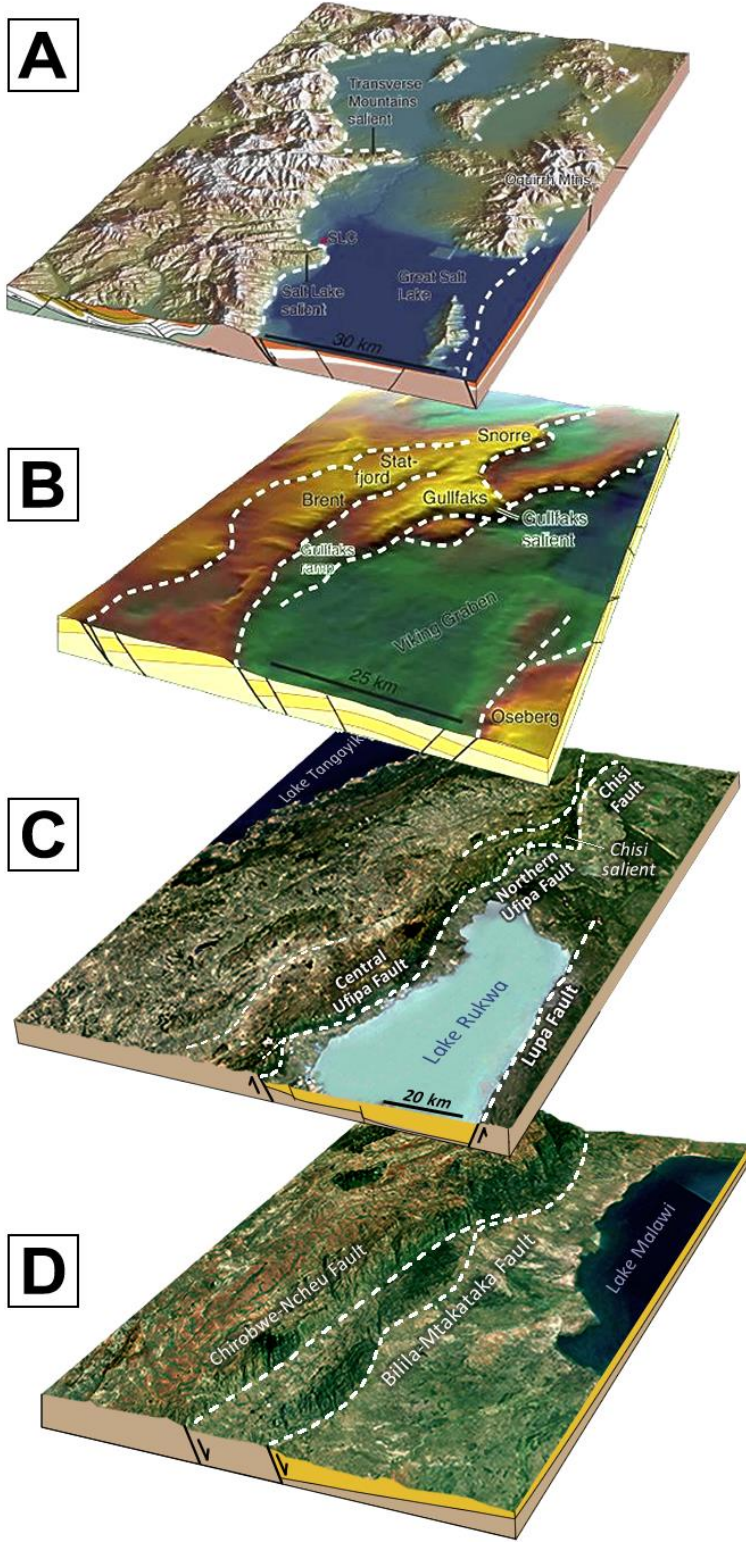
Fig. 16. (A-B) The Wasatch Fault in the Salt Lake area, Utah, and the first-order faults in the northern North Sea (base Cretaceous unconformity) showing concave-curvilinear fault geometries (modified after Fossen and Rotevatn, 2016). (C) Strikingly similar Concave-curvilinear fault geometry occurs in the northern Ufipa Fault and Chisi Fault in the Rukwa Rift. However, the Central Ufipa Fault shows convex-curvilinear fault geometry. (D) The Bilila-Mtakataka Fault also shows excellent convex curvilinear fault geometries.
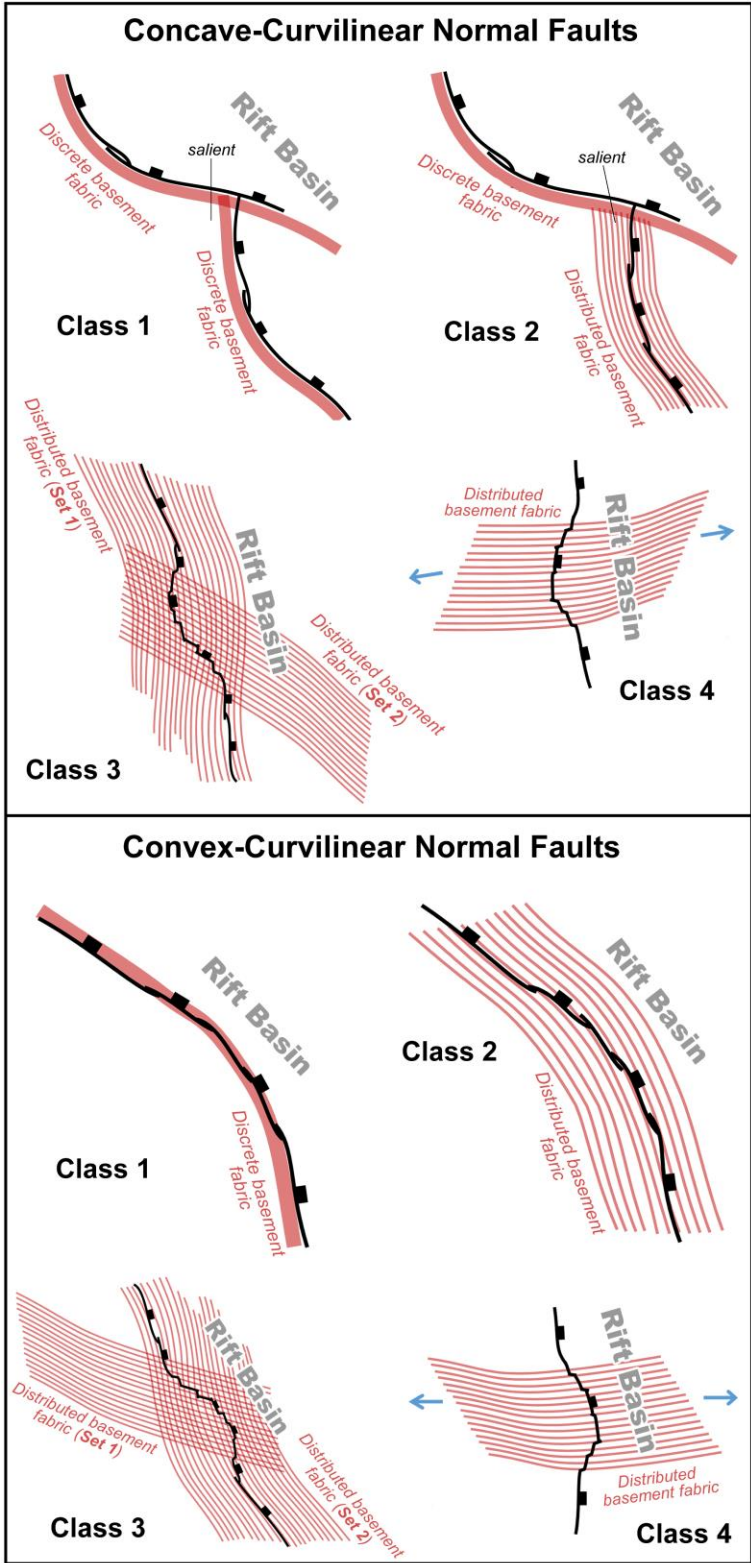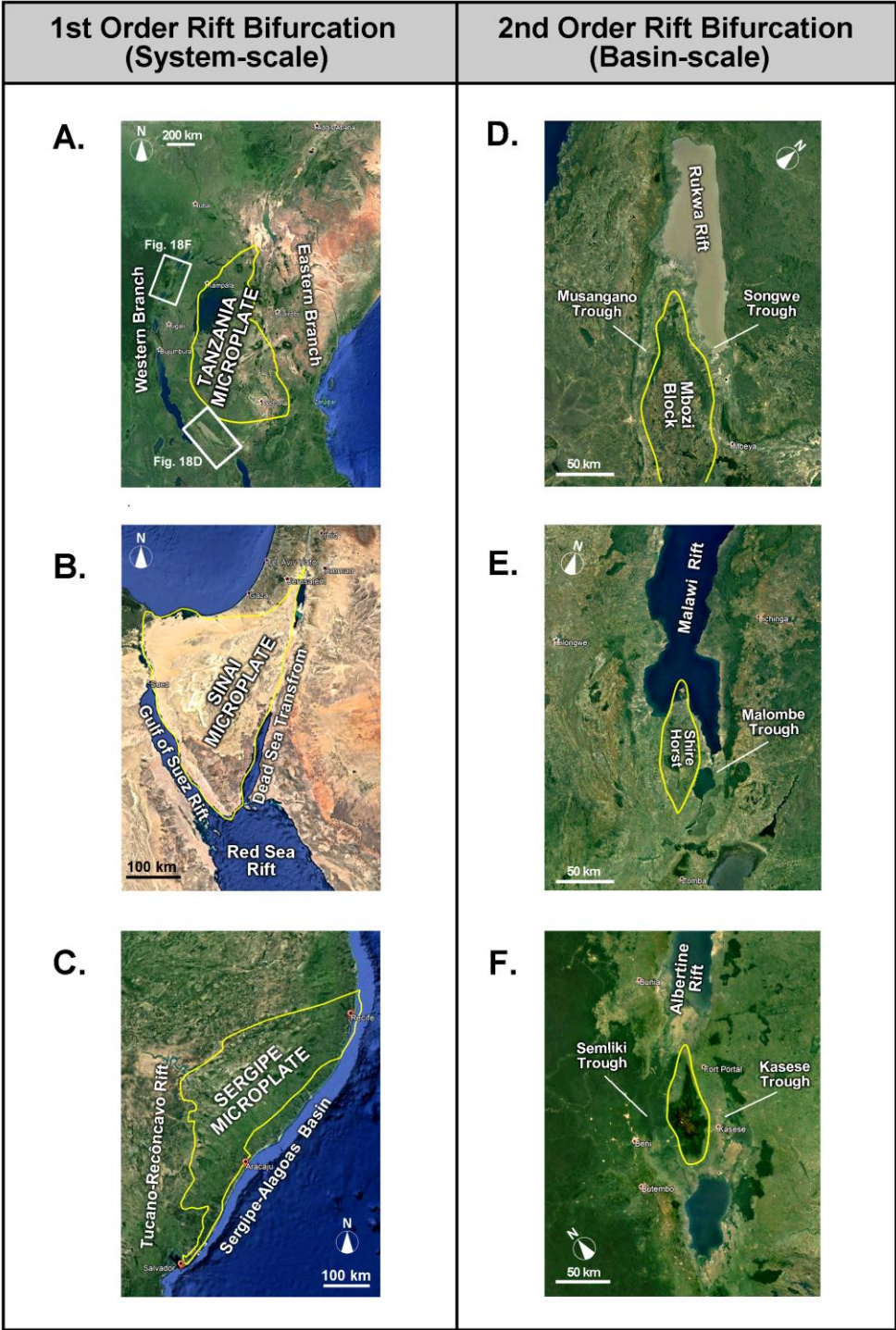
Fig. 17. Models illustrating the control of varying configurations of pre-existing basement fabrics on the development of concave- and convex-curvilinear normal fault plan-view geometries. These models are based on the observations from the Rukwa – North Malawi Rift Segment (this study).

Fig. 18. Examples of system-scale rift bifurcation in the (A) East African Rift System, (B) Red Sea Rift and (C) South Atlantic Rift; and examples of basin-scale rift bifurcation in the (D) Rukwa Rift (see Fig. 18A for location), (E) southern Malawi Rift and (F) Albertine Rift (see Fig. 18A for location). These examples show that the 2nd order bifurcations are integral components of inter-rift transfer zones where the coupling of rift segments take place.